In Vivo Rescue of Cardiomyopathy Through Cardiac Prime Editing

Authors: Wenjing Liang[1†], Lindsey M. Rollosson[1†], Emilee Easter[1], Huanyu Zhou[1], Cristina Dee-Hoskins[1], Amara Greer-Short[1], Timothy Hoey[1], Laura M. Lombardi[1], Kathryn N. Ivey[1], Ze Cheng[1*]

Affiliations:

[1]Tenaya Therapeutics, South San Francisco, CA, USA

†These authors contributed equally

*Corresponding author. Email: zcheng@tenayathera.com

ABSTRACT

Heart disease affects millions of individuals and prime editing (PE) may enable curative therapies that address the underlying drivers of heart disease. Here we describe the establishment and optimization of an *in vivo* cardiac PE platform which mediates efficient editing in the heart with no detectable editing in the liver. We performed a proof-of-concept test on RNA binding motif protein 20 *(RBM20)*, which if mutated, can cause dilated cardiomyopathy (DCM) in humans. Our dual-AAV based PE therapeutic rescued cardiomyopathy phenotypes in the heterozygous *Rbm20*^{R636Q} mouse model. To further develop PE targeting human *RBM20*, we introduced a novel humanized mouse model carrying human *RBM20* wildtype (WT) or R634Q mutant sequences and displaying *RBM20* cardiomyopathy phenotypes. Our human *RBM20* PE therapeutic efficiently corrected the pathogenic mutation and rescued phenotypes in the humanized *RBM20* mouse model. Our findings demonstrate the potential of *in vivo* cardiac PE in

23 treating heart disease, offer a valuable humanized DCM mouse model for developing various
24 therapies, and present an optimized *in vivo* PE platform that can be adopted for targeting other
25 organs and tissues.

26

27 **INTRODUCTION**

28 Heart disease is the leading cause of death in the world, and the unmet need for curative
29 therapies that target the underlying causes of heart disease is high*(1)*. Heart disease comes in
30 many forms, affects individuals at many ages, and can be a result of many factors, including
31 cardiomyocyte malfunction caused by genetic mutations*(2)*.

32 Gene editing technologies may correct the underlying genetic causes of cardiac conditions and
33 base editing (BE) has been developed for treating heart disease in mouse models*(3–9)*, but its
34 therapeutic application is restricted by limited conversion types, the necessity for a nearby PAM
35 sequence, and unintended bystander editing*(3, 10)*. In contrast, PE has the potential to be a
36 transformative therapeutic platform for treating genetic cardiomyopathies due to its ability to
37 mediate precise targeted insertions, deletions, and all 12 possible classes of point mutations in a
38 relatively wide editing window*(10–12)*, however, *in vivo* PE technology has not previously been
39 engineered for efficient and selective editing in cardiomyocytes following systemic
40 administration and the efficacy of *in vivo* PE in treating heart disease has not previously been
41 demonstrated.

42 PE utilizes a fusion protein machinery consisting of a programmable nickase and an engineered
43 reverse transcriptase, guided by a prime editing guide RNA (pegRNA) to the target for
44 installation of the desired edit*(11)*. Optionally, a second guide RNA, the nicking guide RNA

45 (ngRNA), can be included in the PE system to enhance editing efficiency*(11)*. For PE to be
46 translated into cardiac therapeutics that correct pathogenic mutations *in vivo* in cardiomyocytes
47 following systemic administration, methods of arranging PE components in a clinically validated
48 delivery system and efficiently targeting cardiomyocytes are needed. Previous reports introduced
49 dual-AAV PE designs and demonstrated editing and/or efficacy of *in vivo* PE in the liver, the
50 brain, or the retina in relevant mouse models*(13–20)*. Among these studies, Davis et al. and Wei
51 et al. performed systemic administration and showed that v3em PE-AAV system and split-PE-
52 367 system efficiently edited the liver, while the editing efficiency in the heart was
53 suboptimal*(15, 17)*.

54 *RBM20* encodes a splicing regulator and mutations in *RBM20* can cause DCM, accounting for
55 2% to 6% of cases of familial DCM and displaying high penetrance and aggressive progression
56 with high rates of heart failure, arrhythmias, and sudden cardiac death*(21, 22)*. Many *RBM20*
57 disease-causing mutations cluster in a small arginine/serine-rich region*(21, 22)*, which may
58 enable addressing various *RBM20* mutations by a single PE drug*(10, 12)*. These features make
59 *RBM20* an appealing, proof-of-concept target for *in vivo* cardiac PE.

60 In this study, we engineered and optimized *in vivo* PE for cardiomyocyte editing post systemic
61 administration. When tested at the mouse *Rbm20* locus, our PE therapeutic resulted in efficient
62 editing in cardiomyocytes and rescued cardiomyopathy phenotypes in the heterozygous
63 $Rbm20^{R636Q}$ (corresponding to human $RBM20^{R634Q}$ mutation) DCM mouse model*(3)*,
64 representing, to our knowledge, the first demonstration of *in vivo* PE efficacy in cardiac
65 indications. Additionally, we report a novel humanized mouse model carrying human WT or
66 R634Q mutant sequences in and flanking the *RBM20* mutational hotspot region. This humanized
67 model exhibits *RBM20* cardiomyopathy phenotypes and enables *in vivo* testing of PE targeting

human *RBM20*. Finally, we demonstrated that our human *RBM20* PE therapeutic efficiently corrected the pathogenic mutation in the heart, rescued phenotypes in our humanized *RBM20* mouse model, and exhibited no detectable editing in the liver. Our study establishes an *in vivo* cardiac PE platform and exemplifies its therapeutic potential.

RESULTS

A dual-AAV based strategy is established and enables *in vivo* cardiac PE

To express prime editor protein *in vivo* in cardiomyocytes, we employed a 400bp human *TNNT2*-derived promoter which has been shown to mediate strong and cardiac selective gene expression*(23)*. We chose the 1024-CFP intein-split PEmax DRNase-H design (split-PE) for dual-AAV based delivery*(15)*. While Davis et al. arranged the pegRNA and the ngRNA transcription units both in the second, C-terminal AAV cassette (PE-C) and used human U6 and mouse U6 promoters for pegRNA and ngRNA, respectively, to avoid long stretches of homology on a single AAV genome that can lead to recombination*(15)*, the compact size of our *TNNT2*-derived promoter enabled inclusion of the ngRNA transcription unit in the first, N-terminal AAV cassette (PE-N) and use of human U6 promoter for both guide RNAs (Fig. 1A).

To assess *in vivo* cardiac editing efficiency, we chose a previously published pegRNA/ngRNA pair targeting the mouse *Dnmt1* locus*(15)* (Table S1) and packaged the PE cassettes in TNC734 capsid, an in-house engineered capsid with enhanced *in vivo* cardiomyocyte tropism in mouse following systemic administration (Fig. S1, A and B). Administered at 4.6E13 vg/kg per vector in 3.5-week-old mice via retro-orbital (RO) injection, our prototype PE editor showed 21.9% edited

89 next-generation sequencing (NGS) reads at the *Dnmt1* locus in the heart, providing proof of
90 concept for dual AAV vector-based *in vivo* cardiac PE (Fig. 1B).

91 We then applied our prototype to a disease-relevant locus, the corresponding human mutational
92 hotspot in mouse *Rbm20*, and mimicked the real word application by designing a longer reverse
93 transcription template in pegRNA that has the potential to cover the whole hotspot and to correct
94 various pathogenic mutations ("mRbm20-PE prototype"). Carrying in-house optimized guide
95 RNAs (Table S1), mRbm20-PE prototype functions *in vitro* but showed a lower editing
96 efficiency compared to PE at the *Dnmt1* locus (Fig. S1, C to E). Consistent with *in vitro* results,
97 our mRbm20-PE prototype edited the mouse *Rbm20* locus *in vivo* with 5.51% of reads carrying
98 the desired edit when assessed from heart DNA (Fig. 1C and Fig. S1F), less efficiently than PE at
99 the *Dnmt1* locus. It is worth noting that the expression of our prime editor is cardiomyocyte-
100 selective due to the use of *TNNT2*-derived promoter, but genome copies from all cardiac cell
101 types (including cells in which prime editor is not expressed) were collected and contributed to
102 the denominator in our DNA-based analysis, which can cause underestimation of editing
103 efficiency*(3, 4)*. *Rbm20* is also primarily expressed in cardiomyocytes and *Rbm20* RNA
104 transcripts recovered from whole heart lysate mainly originate from cardiomyocytes, so we
105 reasoned that measuring *Rbm20* editing efficiency at the RNA level should better reflect the
106 actual efficiency of our cardiomyocyte-selective PE design*(3, 4)*. Our mRbm20-PE prototype
107 yielded 22.9% desired editing in *Rbm20* RNA transcript analysis (Fig. 1C and Fig. S1G). In this
108 (Fig. S1H) and other experiments (reported later in this manuscript), editing efficiency measured
109 at the RNA level was consistently 4- to 5-fold of the efficiency measured at the DNA level for a
110 cardiomyocyte-specific gene locus, which implies that around 20% to 25% of all genome copies
111 recovered in our whole heart DNA extraction originated from cardiomyocytes. Thus, our

prototype reaches near maximal cardiomyocyte editing at *Dnmt1* locus at this condition (21.9% edited in DNA-based analysis, Fig. 1B); however, our *in vivo* cardiac PE still needed optimization to enhance editing in more challenging settings, such as the *Rbm20* case.

To improve PE efficiency, we fused the RNA-binding, N-terminal domain of the small RNA-binding exonuclease protection factor La to the prime editing protein machinery*(24)*. The resulting design, V19, functions *in vitro* and still allows for dual-AAV packaging (Fig. 2A and Fig. S1, C, D, E, I, and J). To avoid maxing out *in vivo* cardiac editing efficiency and allow head-to-head comparison of the prototype and V19 at the *Dnmt1* locus, we lowered the dosage to 1E13 vg/kg per vector and observed higher editing efficiency by V19 (17.5%) compared to the prototype (11.8%) in *Dnmt1* heart DNA analysis (Fig. 2B).

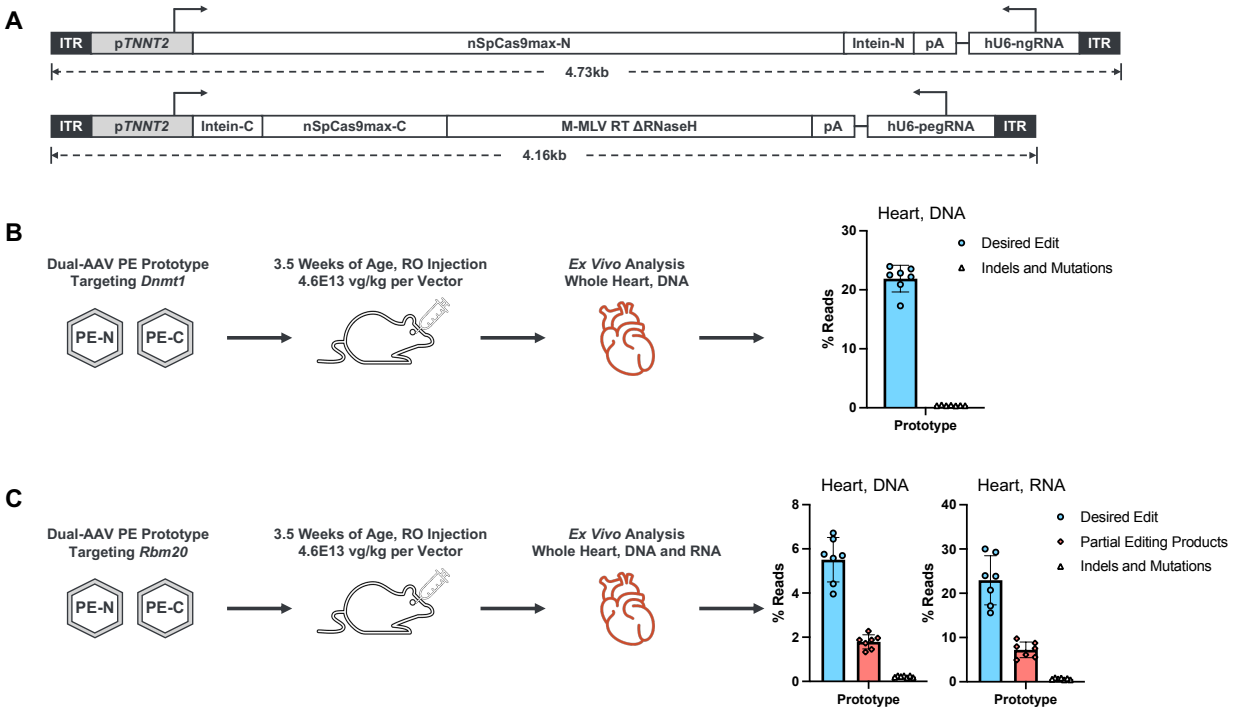

Fig. 1. Establishing a dual-AAV based strategy for *in vivo* cardiac PE. (**A**) Schematic of our prototypical design of dual-AAV based PE cassettes. (**B**) *In vivo* cardiac editing at *Dnmt1* locus by the prototype. (**C**) *In vivo* cardiac editing at *Rbm20* locus by the prototype. PE-N and PE-C cassettes were

126 packaged in TNC734 capsid. Seven mice were enrolled per group. *Ex vivo* editing analysis was performed
127 at 17 weeks post-injection. Dots represent individual mice and error bars represent mean ± SD.

128

129 **_In vivo_ cardiac PE improves heart function of mouse _Rbm20^{R636Q}_ DCM model**

130 We next performed an *in vivo* editing efficiency and efficacy study in *Rbm20*$^{R636Q/+}$ mice, an
131 established model of human *RBM20* cardiomyopathy corresponding to human *RBM20*^{R634Q}
132 mutation*(3)*, to compare mRbm20-PE V19 against mRbm20-PE prototype and assess the
133 therapeutic potential of *in vivo* cardiac PE (Fig. 2C). We used TNC755 capsid (Fig. S1, A and B)
134 in this and all following *in vivo* experiments described in the manuscript. Prior to RO
135 administration at 4.6E13 vg/kg per vector dosage at 3.5 weeks of age, baseline
136 echocardiographic (Echo) analyses were performed in *Rbm20*$^{R636Q/+}$ mice and in age-matched
137 wildtype (WT) controls, and their cardiac function was subsequently monitored by Echo at 4-
138 week intervals up to 20 weeks post-injection, followed by *ex vivo* analyses (Fig. 2C).

139 Vehicle treated *Rbm20*$^{R636Q/+}$ mice exhibited reduced ejection fraction and enlarged left ventricle
140 internal diameters compared to WT mice (Fig. 2, D and E), consistent with the DCM phenotypes
141 reported by Nishiyama et al*(3)*. Both mRbm20-PE prototype and mRbm20-PE V19 treatments
142 improved ejection fraction (Fig. 2, D and F) and mitigated cardiac dilation (Fig. 2, E and G) over
143 time. The rescue of heart function and dilation trended better in mRbm20-PE V19 treated mice
144 compared to mRbm20-PE prototype treated mice (Fig. 2, D to G). Consistently, *ex vivo* editing
145 efficiency analysis detected on average 39.1% and 24.2% of mouse *Rbm20* transcripts carrying
146 the desired edit in the hearts of mRbm20-PE V19 and mRbm20-PE prototype treated mice,
147 respectively (Fig. 2H and Fig. S2, A to C). *Ex vivo* splicing analysis of RBM20 downstream

148 targets Titin (*Ttn*) and calcium/calmodulin dependent protein kinase II delta (*Camk2d*) revealed
149 partial rescue of abnormal splicing patterns*(3, 25)* by mRbm20-PE V19 and mRbm20-PE
150 prototype treatment (Fig. 2I and Fig. S2D).

151 The heterozygous genotype of *Rbm20*$^{R636Q/+}$ mice complicates the interpretation of editing
152 efficiency as both *Rbm20*^{R636Q} and *Rbm20* WT alleles can be recognized and edited to the same
153 final sequence by mRbm20-PE, and we cannot directly measure the percentage of mutant allele
154 copies corrected in NGS analysis. The relative abundance of unedited mutant and WT allelic
155 sequences stays roughly unchanged (close to 1:1 ratio) in our mRbm20-PE studies regardless of
156 whether PE was performed (Fig. S1G and Fig. S2A), suggesting that our mRbm20-PE editors
157 edit *Rbm20*^{R636Q} and *Rbm20* WT alleles at similar efficiencies and the overall percentage of
158 desired edit observed in our NGS analysis is a close approximation of the percentage of mutant
159 allele copies corrected.

160 Together, these results demonstrate the improvement of V19 design over the prototype and
161 support the therapeutic potential of *in vivo* cardiac PE; however, unedited *Rbm20*^{R636Q} allelic
162 sequence still accounted for 33.8% of all reads in NGS analysis of mRbm20-PE V19 treated
163 mice, which translates to nearly 70% of cardiomyocytes still carrying the uncorrected mutant
164 allele, prompting us to further optimize the *in vivo* PE design.

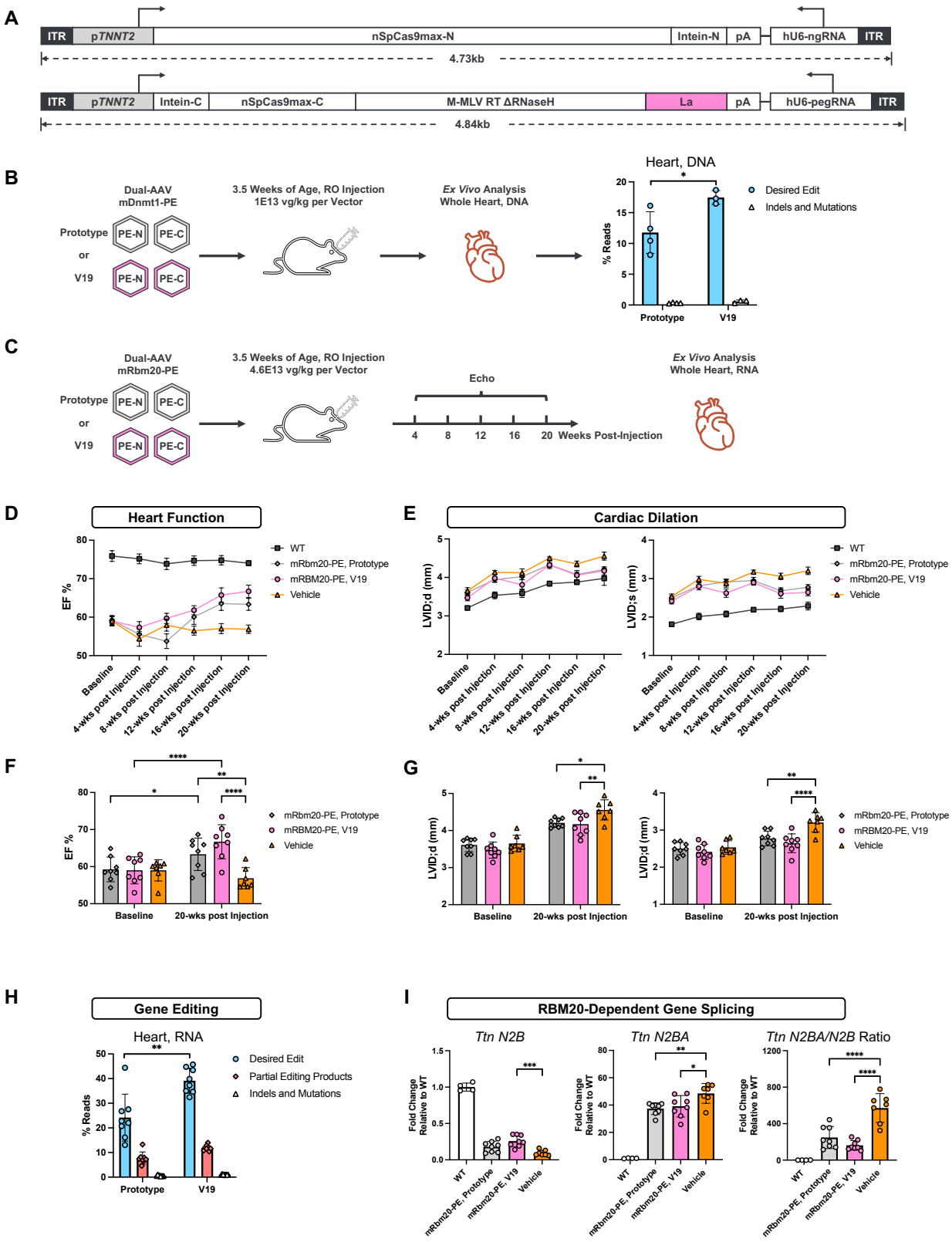
A
ITR
pTNNT2
nSpCas9max-N
Intein-N
pA
hU6-ngRNA
ITR
4.73kb
ITR
pTNNT2
Intein-C
nSpCas9max-C
M-MLV RT ΔRNaseH
La
pA
hU6-pegRNA
ITR
4.84kb
B
Dual-AAV
mDnmt1-PE
Prototype
or
V19
PE-N
PE-C
3.5 Weeks of Age, RO Injection
1E13 vg/kg per Vector
Ex Vivo Analysis
Whole Heart, DNA
Heart, DNA
% Reads
Desired Edit
Indels and Mutations
Prototype
V19
C
Dual-AAV
mRbm20-PE
3.5 Weeks of Age, RO Injection
4.6E13 vg/kg per Vector
Echo
4 8 12 16 20 Weeks Post-Injection
Ex Vivo Analysis
Whole Heart, RNA
D
Heart Function
EF %
WT
mRbm20-PE, Prototype
mRBM20-PE, V19
Vehicle
Baseline
4-wks post Injection
8-wks post Injection
12-wks post Injection
16-wks post Injection
20-wks post Injection
E
Cardiac Dilation
LVID;d (mm)
LVID;s (mm)
F
EF %
Baseline
20-wks post Injection
G
LVID;d (mm)
H
Gene Editing
Heart, RNA
% Reads
Desired Edit
Partial Editing Products
Indels and Mutations
I
RBM20-Dependent Gene Splicing
Ttn N2B
Ttn N2BA
Ttn N2BA/N2B Ratio
Fold Change
Relative to WT

166 **Fig. 2. V19 mediates greater *in vivo* cardiac editing efficiency than the prototype and rescues**
167 **phenotypes in *Rbm20*^{R636Q} mouse model.** (**A**) Schematic of V19 design. (**B**) *In vivo* cardiac editing at the
168 *Dnmt1* locus by the prototype and V19. PE cassettes were packaged in TNC734 capsid. Three to four
169 mice were enrolled per group. *Ex vivo* editing analysis was performed at 3 weeks post-injection. (**C**)
170 Schematic design of *in vivo* editing efficiency and efficacy study testing mRbm20-PE prototype and V19
171 in *Rbm20*^{R636Q} mouse model. PE cassettes were packaged in TNC755 capsid. Seven to eight mice were
172 enrolled per group. (**D** to **G**) Ejection fraction (EF) measurements (D and F) by Echo and left ventricle
173 internal diameter measurements (E and G) at diastolic stage (LVID;d) and at systolic stage (LVID;s). For
174 D and E, error bars represent mean ± SEM. (**H**) Editing efficiency at the *Rbm20* locus, detected from
175 whole heart RNA samples. (**I**) Splicing patterns of *Ttn* gene. For B and H, dots represent individual mice,
176 error bars represent mean ± SD, statistical significance was calculated using unpaired t-test. For E, G, and
177 I, dots represent individual mice, error bars represent mean ± SD, statistical significance was calculated
178 using two-way ANOVA with Tukey's multiple comparisons test. For B and F to I, *$P < 0.05$, **$P < 0.01$,
179 ***$P < 0.001$, ****$P < 0.0001$.

180

181 **Further optimization improves *in vivo* cardiac PE efficiency**

182 While Yan et al. showed that fusing the RNA-binding domain of La to the C-terminus of PE
183 protein, namely PE7, was the most efficient among all fusing locations tested*(24)*, we found that
184 fusing the RNA-binding domain internally between Cas9 and M-MLV RT DRNase-H showed
185 improved efficiency over V19, which has the C-terminal fusion arrangement, under our split-PE
186 setting. We name this new design V20 (Fig. 3A and Fig. S1, C, D, E, I, and J). When tested *in*
187 *vivo* at 2.8E13 vg/kg per vector, V20 more than doubled cardiac editing efficiency compared to
188 V19 at the mouse *Rbm20* locus (74.5% versus 34.5%, measured at RNA transcript level) (Fig.
189 3B and Fig. S3A).

190 In parallel, we explored alternative reverse transcriptases developed by Doman et al*(26)*. By
191 swapping M-MLV RT DRNase-H in V19 to evolved Tf1 RT and evolved and engineered Tf1 RT
192 (used in PE6b and PE6c, respectively, in Doman et al.), we developed V22 and V24, respectively
193 (Fig. 3A and Fig. S1, C, D, E, I, and J). While V22 yielded 50.8% of mRbm20 RNA transcripts
194 carrying the desired edit *in vivo* in mouse heart, V24 showed 77.1% editing, comparable to V20
195 and more than doubled compared to V19 (Fig. 3B and Fig. S3A).

196 Furthermore, we combined the internal fusion arrangement of La of V20 with the alternative
197 reverse transcriptases in V22 and V24. The resulting PE designs, V27 and V28, functioned well
198 *in vitro* (Fig. S1, C, D, E, I, and J).

199 Finally, long-term exposure to PE activity may not always be beneficial and in certain cases,
200 inactivation of PE expression and/or function post-administration may be desirable. To this end,
201 we propose a strategy of PE self-inactivation (SI) (Fig. S3B) and provide an *in vivo* proof-of-
202 concept demonstrating editing at both the genomic target and the SI site (Fig. S3, C and D).

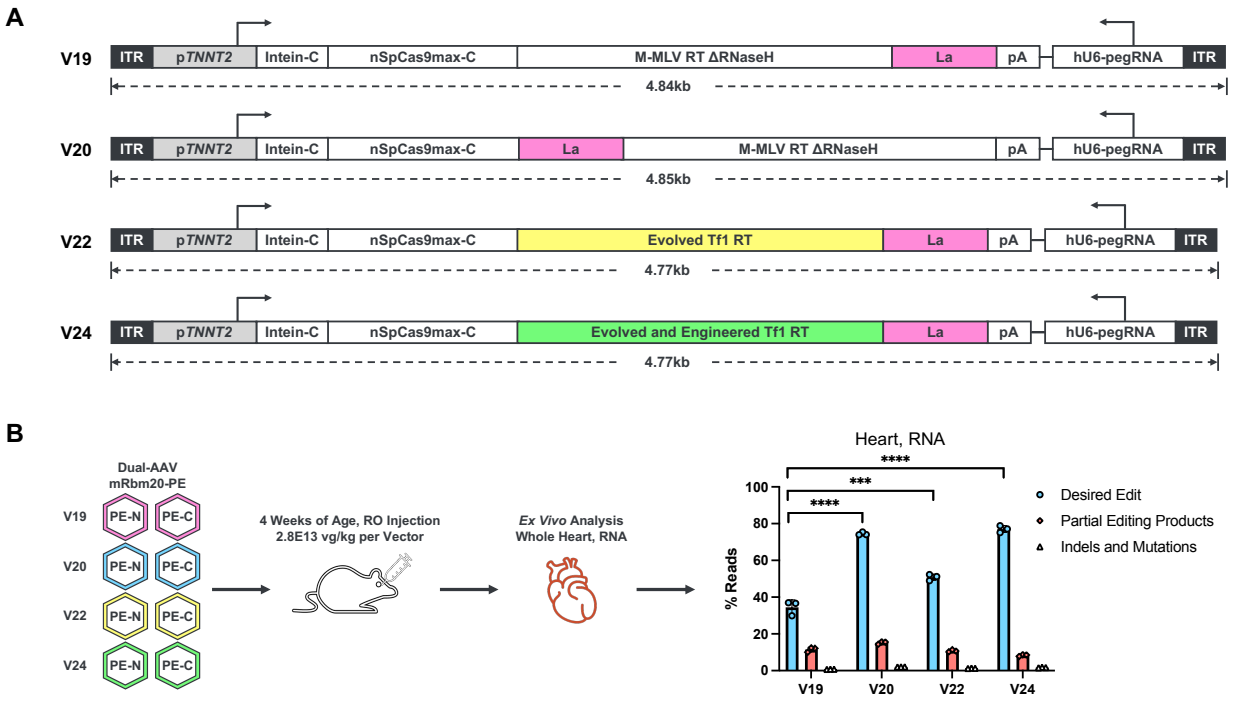

Fig. 3. Further optimization enhances *in vivo* cardiac editing efficiency. (**A**) Schematics of V19, V20, V22, and V24 designs. (**B**) *In vivo* cardiac editing at the *Rbm20* locus by mRBM20-PE V19, V20, V22, and V24. WT C57BL/6J mice were used in this study. *Ex vivo* analysis was performed at 8 weeks post-injection. Dots represent individual mice, error bars represent mean ± SD, statistical significance was calculated using one-way ANOVA with Tukey's multiple comparisons test. ***$P < 0.001$, ****$P < 0.0001$.

A novel humanized *RBM20* mouse model displays *RBM20* cardiomyopathy phenotypes

Having demonstrated the therapeutic potential of *in vivo* cardiac PE and having identified PE designs with enhanced *in vivo* efficiency, we sought to apply this platform to treating human pathogenic mutations. However, the differences at the nucleotide sequence level of orthologous genes in different species often impede testing of human gene targeting PE in animal models. We overcame this challenge by designing and generating a novel humanized *RBM20* mouse model.

The *RBM20* mutational hotspot region is located near the beginning of exon 9. Taking advantage of the high conservation between human RBM20 and mouse Rbm20 protein sequences in and flanking the mutational hotspot region, we replaced 64 base pairs (bp) at the 5' start of exon 9 of mouse *Rbm20* with the corresponding sequence of human *RBM20* (Fig. 4 and Fig. S4A). Additionally, we humanized the last 200 bp of intron 8, making the total humanized region to 264-bp-long, which allows binding by pegRNAs and ngRNAs designed for human *RBM20* editing. To enable disease modeling and *in vivo* efficacy testing, we constructed two lines carrying humanized *RBM20* WT sequence or humanized $RBM20^{R634Q}$ sequence (human RBM20 amino acid position numbering is used here to avoid confusion, despite that the actual mutation position is 636 in the human-mouse chimeric gene) (Fig. 4 and Fig. S4A), and further generated heterozygous $hRBM20^{R634Q}/hRBM20^{+}$ mice by crossing these two humanized lines, confirmed by genotyping and Sanger sequencing (Fig. S4B).

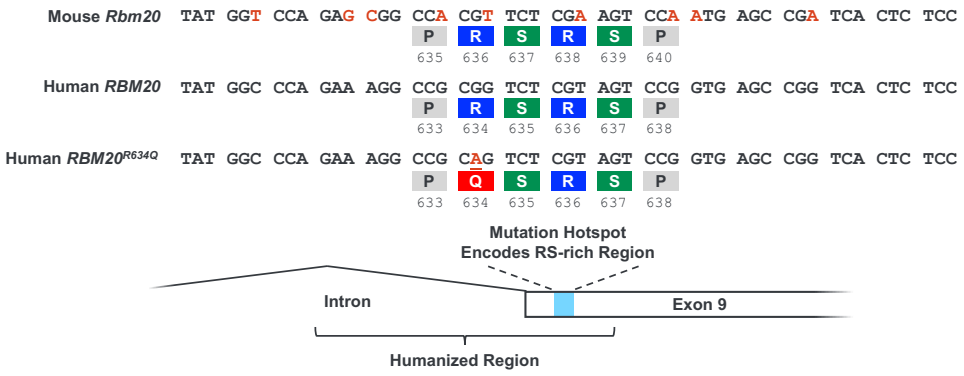

Fig. 4. Design and generation of a partially humanized *RBM20* mouse model. Schematic of the design of our humanized *RBM20* mouse model, highlighting the sequence differences between mouse and human, and the location of the humanized region.

234 To characterize this newly generated mouse model, we conducted comprehensive phenotypic
235 assessments. Echo revealed that while humanized WT controls remained healthy, heterozygous
236 mutant mice (*hRBM20*^{R634Q}*/hRBM20*$^{+}$) developed a moderate DCM phenotype with reduced
237 ejection fraction (EF) and increased left ventricular internal diameter in systole (LVID;s) and
238 diastole (LVID;d) (Fig. 5, A and B). Homozygous mutants (*hRBM20*^{R634Q}*/hRBM20*^{R634Q}*)*
239 exhibited severe heart failure and ventricular enlargement (Fig. 5, A and B). Notably, the
240 homozygous mice showed significantly increased heart weight to body weight (HW/BW) ratios
241 (Fig. 5C) and a shortened lifespan (<3 months) (Fig. 5D). Visualization of freshly excised
242 cardiac tissue and H&E-stained heart slices revealed dilation in 22-week-old heterozygous
243 mutant mice (Fig. 5, E and F). Masson's trichrome staining showed no notable fibrosis (Fig. 5G).
244 Molecular analysis confirmed abnormal splicing of *Ttn* (increased N2BA isoform, decreased
245 N2B isoform; Fig. 5H) and *Camk2d* (increased Camk2d-A, decreased B/C isoforms; Fig. 5I) in
246 mutant hearts. Additionally, the expression levels of heart failure markers natriuretic peptide A
247 and B (*Nppa* and *Nppb*), as well as the fibrosis-associated gene transforming growth factor, beta
248 (*Tgf-β*), were modestly increased in heterozygous hearts (Fig. S5, A and B). Electrocardiogram
249 (EKG) analysis did not reveal any significant differences between mutant and wild-type mice
250 (Fig. S5C). Overall, our novel humanized *RBM20* mouse model exhibits *RBM20*
251 cardiomyopathy phenotypes reminiscent of those observed in mouse endogenous *Rbm20* disease
252 model and human patients*(3, 27)*, and provides a valuable platform for evaluating the functional
253 consequences of human *RBM20* mutation in a physiological context and for testing PE targeting
254 human *RBM20*.

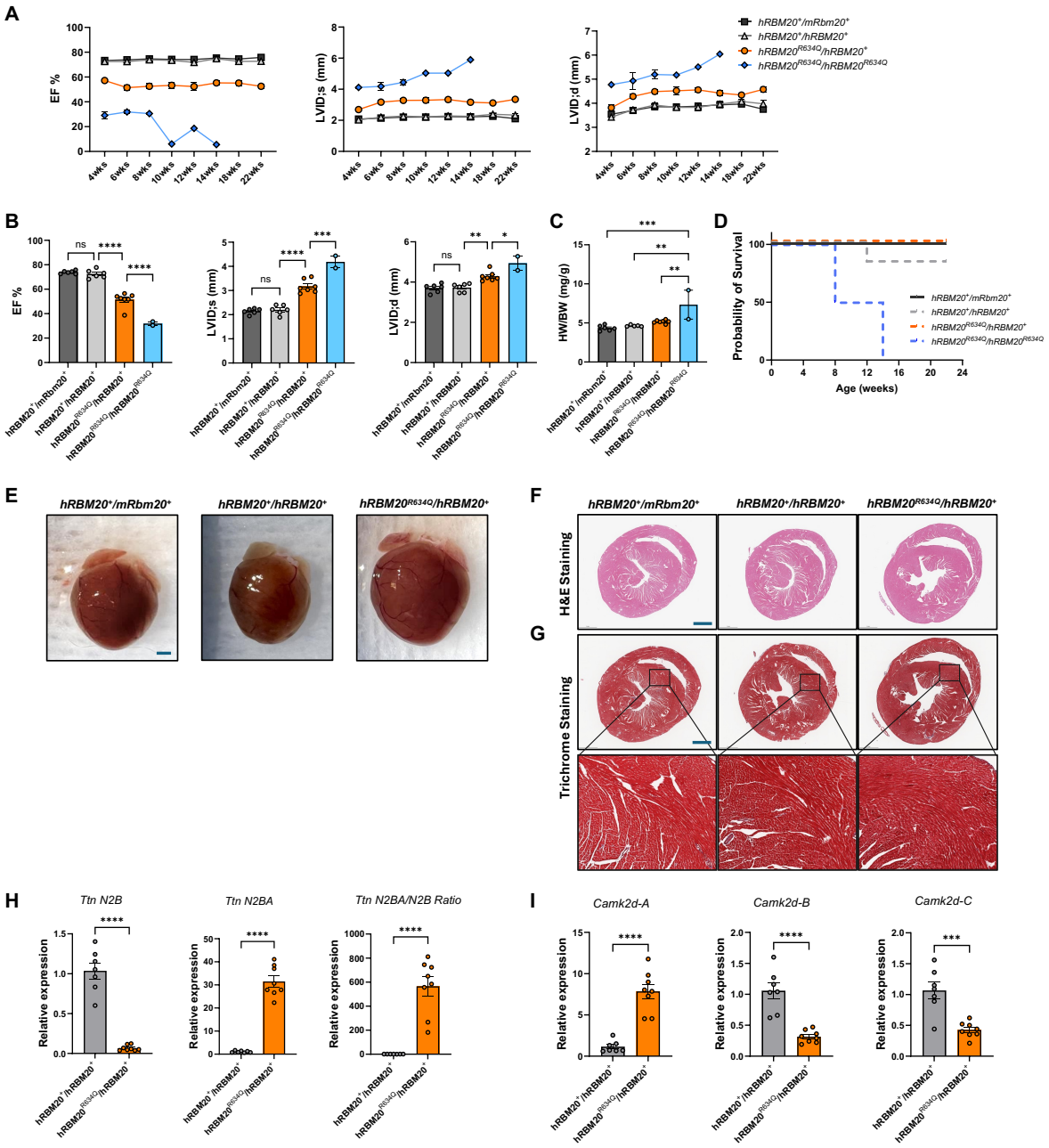

255

256 **Fig. 5. Humanized *RBM20*^{R634Q} mice show DCM phenotype**. (**A**) Cardiac function progression of

257 heterozygous humanized WT *(hRBM20*$^{+}$*/mRbm20*$^{+}$*)* (n=6), homozygous humanized WT

258 *(hRBM20*$^{+}$*/hRBM20*$^{+}$*)* (n=6), heterozygous mutant *(hRBM20*^{R634Q}*/hRBM20*$^{+}$*)* (n=7), and homozygous

259 mutant *(hRBM20*^{R634Q}*/hRBM20*^{R634Q}*)* (n=2). (**B**) Ejection fraction (EF), left ventricle internal diameter at

260 systolic stage (LVID;s) and left ventricular internal diameter at diastolic stage (LVID;d) at 6 weeks of age.

261 (**C**) Heart weight to body weight ratios (HW/BW) at death (animals died during the study) or at 22 weeks
262 of age. For **b** and **c**, dots represent individual mice. For A to C, error bars indicate mean ± SEM. and
263 statistical significance was calculated using one-way ANOVA with Tukey's multiple comparisons test.
264 (**D**) Mortality over time. (**E**) Representative whole-heart images. (**F**) Representative hematoxylin and
265 eosin (H&E)–stained heart sections. (**G**) Representative Masson's trichrome–stained heart sections (n =
266 5–7 per group). For E to G, scalebar = 1 mm. (**H**) Splicing patterns of *Ttn*. (**I**) Splicing patterns of
267 *Camk2d*. For H and I, dots represent individual mice, error bars indicate mean ± SEM., and statistical
268 significance was calculated using unpaired t-test. For B, H, I, *$P < 0.05$, **$P < 0.01$, ***$P < 0.001$,
269 ****$P < 0.0001$.

270

271 ***In vivo* cardiac PE corrects human *RBM20*^{R634Q} mutation and rescues cardiomyopathy**
272 **phenotypes**

273 To evaluate *in vivo* PE of human *RBM20*, we administered PE-hRBM20-4.9 (Table S2), which
274 uses V20 design and carries a pair of human *RBM20*-targeting pegRNA/ngRNA (Table S1)
275 developed and validated *in vitro* (Fig. S1I), to *hRBM20*^{R634Q}*/mRbm20*$^{+}$ mice at 1.5E13, 3E13,
276 and 5E13 vg/kg dosages. *Ex vivo* editing analysis at 4 weeks post-injection detected 16.9%,
277 29.3%, and 32.5% *hRBM20* transcripts fully edited at these three dosages (Fig. S5, D to F),
278 indicating diminishing returns on the editing dose response. PE-hRBM20-4.9 installs a silent edit
279 in addition to the mutation-correcting edit (Fig. S5D) and the design of our mRbm20-PE also
280 followed the same concept (Fig. S1F). This allows us to validate the PE constructs *in vitro* in WT
281 human cells prior to *in vivo* experiments, however, in both cases we observed large amounts of
282 partial editing products with only the silent edit but not the mutation-correcting edit (Fig. 1C,
283 Fig. 2G, Fig. S1F, and Fig. S5, D to F). The proximity to the nick site may make the silent edit

284 more likely to be installed than the mutation-correcting edit (for example, due to premature stop
285 of reverse transcription), and the overlapping of the silent edit with the protospacer adjacent
286 motif (PAM) or spacer binding region may leave silent-edit-only DNA harder to be recognized
287 again and acquire the mutation-correcting edit. Thus, we developed two new *RBM20*-targeting
288 pegRNAs (Table S1) which edit mutant allele to WT sequence without incorporating any silent
289 edit. We validated their performance in mouse embryonic fibroblasts (MEFs) isolated from
290 homozygous $hRBM20^{R634Q}/hRBM20^{R634Q}$ mice and named the resulting PE constructs PE-
291 hRBM20-4.11 and PE-hRBM20-4.12 (Fig. S5G and Table S2).

292 Encouraged by the performance of our human *RBM20* targeting PE constructs and the clear
293 *RBM20* cardiomyopathy phenotypes of our novel humanized mouse model, we performed an
294 efficacy study in which humanized heterozygous $hRBM20^{R634Q}/hRBM20^{+}$ mutant mice were
295 administered systemically with PE-hRBM20-4.9, PE-hRBM20-4.11, or PE-hRBM20-4.12 at
296 3E13 vg/kg at 3.5 weeks of age. Heart function and dilation were monitored by
297 echocardiography prior to dosing and at 4-week intervals for up to 16 weeks post-injection,
298 followed by *ex vivo* editing and gene splicing analyses (Fig. 6A). While vehicle treated
299 $hRBM20^{R634Q}/hRBM20^{+}$ mice displayed reduced ejection fraction and increased left ventricle
300 internal diameters, consistent with model development observations, PE-hRBM20-4.9, PE-
301 hRBM20-4.11, and PE-hRBM20-4.12 treated animals showed better heart function and cardiac
302 dilation compared to the vehicle control (Fig. 6, B to E). PE-hRBM20-4.11 showed the strongest
303 rescue among treated groups, with both ejection fraction and cardiac dilation measurements
304 improved over time trending towards the WT control ($hRBM20^{+}/hRBM20^{+}$) levels (Fig. 6, B to
305 E). Since the desired post-editing product of PE-hRBM20-4.11 and PE-hRBM20-4.12 is
306 identical to and indistinguishable from the pre-existing WT hRBM20 allelic sequence (Fig. S6, A

307 to C), we report the percentages of reads that encode WT hRBM20 protein or R634Q mutant
308 protein in NGS editing analysis of this study. While nearly half (49.0%) of all reads in vehicle
309 treated heterozygous *hRBM20*^{R634Q}*/hRBM20*$^{+}$ mice corresponded to R634Q mutant, PE-
310 hRBM20-4.9, PE-hRBM20-4.11, and PE-hRBM20-4.12 treated groups had on average 27.9%,
311 16.4%, and 17.9% reads, respectively, encoding R634Q mutant protein (Fig. 6, F and G, and Fig.
312 S6C), which can be interpreted as roughly 57%, 33%, and 37% of all cardiomyocytes with the
313 mutant allele remaining unedited. The splicing patterns of RBM20 downstream targets *Ttn* and
314 *Camk2d* were also partially rescued in all three treated groups, with the PE-hRBM20-4.11
315 trending the best (Fig. 6, H and I).

316 Systemic administration of dual-AAV prime editors expressed by ubiquitous promoters leads to
317 high levels of editing in the liver*(15, 17)*. To assess whether our *in vivo* cardiac PE therapeutic
318 shows off-targeting to the liver, we extracted DNA from the liver of PE-hRBM20-4.9, PE-
319 hRBM20-4.11, PE-hRBM20-4.12, and vehicle treated animals and performed editing efficiency
320 analysis. The editing was undetectable at the target locus in the liver of all three treated groups,
321 in contrast to what was observed in heart DNA samples (Fig. S6, D to G). We next investigated
322 deeper into PE-hRBM20-4.9 treated samples in which we can clearly distinguish several post-
323 editing sequences from the pre-existing WT allele thanks to the silent edit introduced by PE-
324 hRBM20-4.9. We saw no detectable change in any post-editing sequence populations (Fig. S6H).

325 Finally, we observed very low levels of indels and undesired mutations in this (1% to 2% of heart
326 RNA reads and 0.2% to 0.5% of heart DNA reads) (Fig. 6F and Fig. S6, C and D) and all
327 previous *in vivo* PE experiments, which is consistent with the observation by Davis et al*(15)*.

328 Together, these results demonstrate that our *in vivo* cardiac PE corrects the pathogenic mutation
329 in the heart and rescues cardiomyopathy phenotypes in our novel humanized *RBM20* mouse
330 model with no detected editing in the liver.

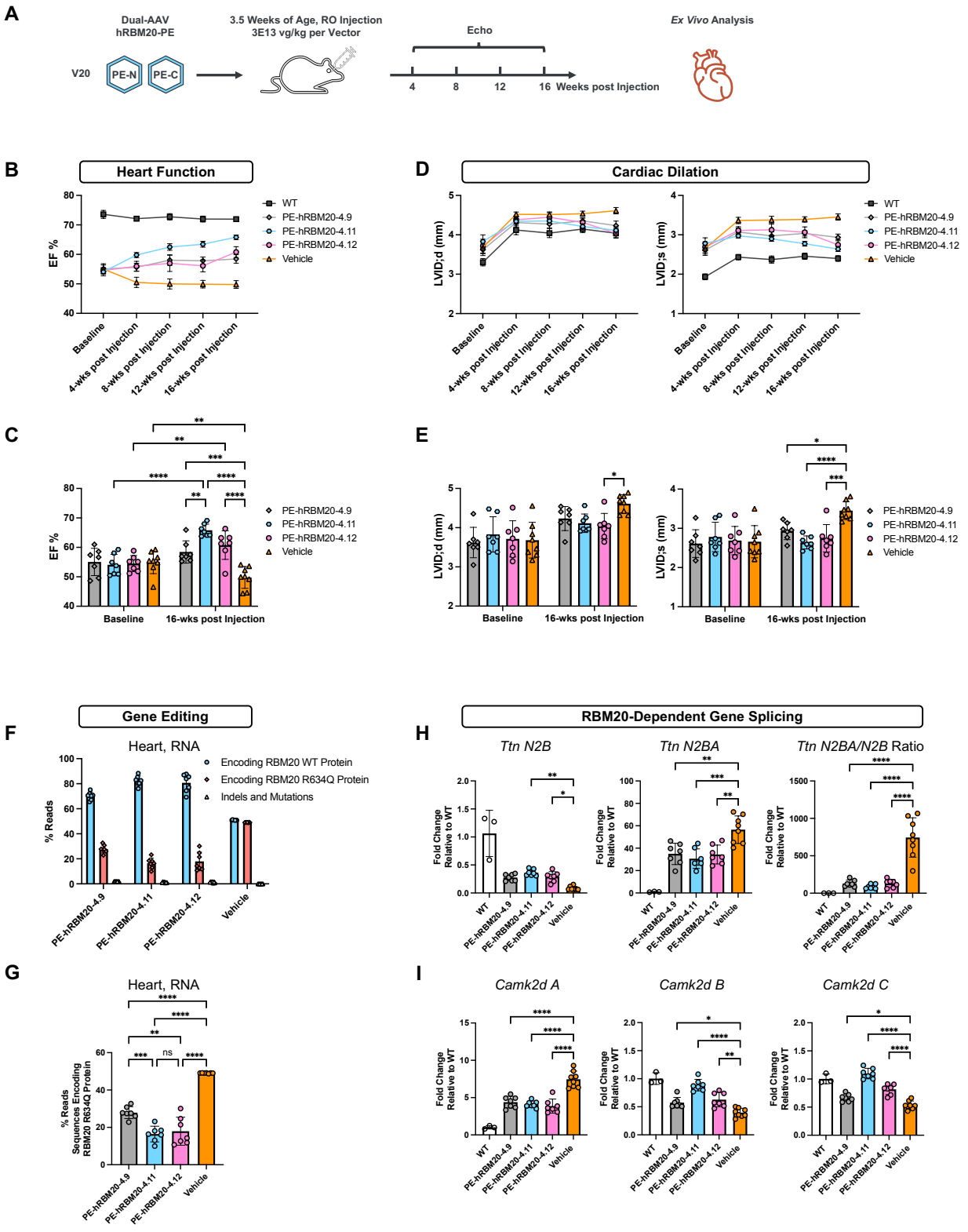
A
Dual-AAV
hRBM20-PE
V20
PE-N
PE-C
3.5 Weeks of Age, RO Injection
3E13 vg/kg per Vector
Echo
4
8
12
16 Weeks post Injection
Ex Vivo Analysis
B
Heart Function
EF %
WT
PE-hRBM20-4.9
PE-hRBM20-4.11
PE-hRBM20-4.12
Vehicle
Baseline
4-wks post Injection
8-wks post Injection
12-wks post Injection
16-wks post Injection
C
EF %
Baseline
16-wks post Injection
D
Cardiac Dilation
LVID;d (mm)
LVID;s (mm)
E
LVID;d (mm)
LVID;s (mm)
F
Gene Editing
Heart, RNA
% Reads
Encoding RBM20 WT Protein
Encoding RBM20 R634Q Protein
Indels and Mutations
G
Heart, RNA
% Reads Sequences Encoding RBM20 R634Q Protein
ns
H
RBM20-Dependent Gene Splicing
Ttn N2B
Ttn N2BA
Ttn N2BA/N2B Ratio
Fold Change Relative to WT
I
Camk2d A
Camk2d B
Camk2d C

331

332 **Fig. 6. PE therapeutic targeting human *RBM20* mediates *in vivo* correction of pathogenic mutation**
333 **in the heart and rescues cardiomyopathy phenotypes in humanized *RBM20*^{R634Q} mouse model.** (**A**)
334 Schematic design of *in vivo* editing efficiency and efficacy study testing PE-hRBM20-4.9, PE-hRBM20-
335 4.11, and PE-hRBM20-4.12 in our novel humanized mouse model. PE cassettes were packaged in
336 TNC755 capsid. Seven to eight mice were enrolled per group. (**B** and **C**) Ejection fraction (EF)
337 measurements by Echo. (**D** and **E**) Left ventricle internal diameter at diastolic stage (LVID;d) and at
338 systolic stage (LVID;s) measurements. (**F** and **G**) Editing efficiency at humanized *RBM20* locus, detected
339 from whole heart RNA samples. (**H**) Splicing patterns of *Ttn*. (**I**) Splicing patterns of *Camk2d*. For B and
340 D, error bars represent mean ± SEM. For C to I, dots represent individual mice, error bars represent mean
341 ± SD. For C and E, statistical significance was calculated using two-way ANOVA with Tukey's multiple
342 comparisons test. For G to I, statistical significance was calculated using one-way ANOVA with Tukey's
343 multiple comparisons test. For C, E, G to I, *$P < 0.05$, **$P < 0.01$, ***$P < 0.001$, ****$P < 0.0001$.

344

345 **DISCUSSION**

346 We present a dual-AAV based *in vivo* cardiac PE platform with designs and optimizations for
347 targeted and efficient *in vivo* PE in cardiomyocytes. Our results suggest that while incorporating
348 the RNA-binding domain of La enhances editing efficiency, the location of La in the fusion
349 protein has a large impact on *in vivo* cardiac PE efficiency, at least for the genomic target locus
350 tested in this study. Replacing MLV RT with Tf1 RT variants also improves editing efficiency,
351 and interestingly, lowered the tendency to generate partially edited products, compared to their
352 counterpart using MLV RT in the mouse *Rbm20* case study where PE installs more than one
353 nucleotide change (Fig. S3A). Future study may investigate whether this trend is consistent
354 across different targets and explore the underlying mechanisms. Additionally, the promising *in*

355 *vitro* results of our V27 and V28 designs, which combine the favorable location of La and Tf1
356 RT variants, warrant future *in vivo* testing.

357 For split-PE to function, both PE-N and PE-C need to be present in the same cell and expressed
358 at a sufficiently high level, posing a high demand for delivery efficiency. Consistently, our in-
359 house engineered cardiac tropic capsids mediated enhanced PE efficiency compared to the same
360 PE design delivered by AAV9, especially at a low dose level (Fig. S1B). Moreover, the efforts of
361 identifying compact nucleases and reverse transcriptases*(26, 28–30)* may enable single-AAV PE
362 in the future, potentially improving efficacy and/or reducing dosage.

363 Although we developed our *in vivo* PE platform aiming at cardiac editing, our PE designs can be
364 adopted for targeting other organs and tissues. Researchers may modify our PE designs by
365 changing the promoter and/or the capsid to those that better fit their organs/tissues of interest.
366 Thus, our PE optimization efforts possess broader impact beyond cardiac indications.

367 Here we use $RBM20^{R634Q}$ mutation as a case study, however, our hRBM20-PE therapeutic was
368 designed to be compatible with various mutations in or near the *RBM20* mutational hotspot
369 region, including but not limited to P633L, R634W, R634Q, S635A, R636C, R636S, R636H,
370 S637G*(21)*, offering an attractive advantage over BE strategies*(3, 4)*. Future *in vitro* and *in vivo*
371 studies should be performed to investigate the editing efficiency of our hRBM20-PE therapeutic
372 on other *RBM20* mutations.

373 In our humanized *RBM20* efficacy study, the heart function and left ventricle dilation were still
374 trending better in two of the treatment groups at the end of in-life observation stage (Fig. 6, B
375 and D). AAV delivery supports long-term transgene expression*(31)*, thus the percentage of
376 unedited mutant *RBM20* copies may continue to decrease over time, which would lead to

377 continuous improvement of efficacy. It is also possible that the phenotypic improvements lag
378 after the correction of mutant *RBM20* copies. Therefore, future editing kinetics investigation may
379 be of interest.

380 Finally, while we employed our novel humanized *RBM20* mouse model for *in vivo* PE testing,
381 this model also enables *in vivo* testing of other sequence-specific therapeutics designed to target
382 the human *RBM20* mutational hotspot, including but not limited to CRISPR/Cas9 editing, BE,
383 antisense oligonucleotides, RNA interference, and CRISPR interference. Additionally, it may
384 serve as a valuable DCM model to test various small molecule and gene replacement drugs.

385 There are some limitations to this work, raising the need of future experiments for our findings to
386 be applied in the clinic. First, we performed *in vivo* editing and efficacy studies in mice and it
387 remains unclear whether our *in vivo* cardiac PE platform can achieve efficient editing in large
388 animals. Investigations in non-human primate models should be pursued. Second, long-term
389 follow-up studies addressing the endurance of efficacy, immune responses, off-targeting,
390 tumorigenesis, etc., were not included in the current research but should be performed prior to
391 clinical translation. In addition, only one dosage was tested in the *RBM20 in vivo* efficacy
392 experiment. It would be a crucial future step to examine the dose response and tolerance of *in*
393 *vivo* cardiac PE therapeutic. Last, we focused on the technological development of *in vivo*
394 cardiac PE and the demonstration of cardiac function improvements in the current study, whereas
395 biological and mechanistic questions, such as the intracellular localization of RBM20 protein and
396 whole transcriptome features pre- and post-treatment, may be of interest in future studies.

397

398 **MATERIALS AND METHODS**

399 **Study design**

400 This study aimed to develop an *in vivo* cardiac PE platform and test its therapeutic potential. This
401 study used *RBM20* cardiomyopathy as a case study to demonstrate the *in vivo* efficacy of our PE
402 platform. Post genotyping, animals were randomized and assigned to experimental groups,
403 aiming at having similar average baseline ejection fraction values and body weight across
404 groups. In efficacy experiments, injection and echocardiography analysis were performed by
405 blinded operators. Each experiment carried biological replicates as indicated in the figures and
406 figure legends.

407

408 **Molecular cloning**

409 Sequences of guide RNAs, plasmids, AAV transgene cassettes, and AAV capsids are available
410 upon request.

411 Plasmids were generated via Gibson assembly or ligation, using NEBuilder HiFi DNA Assembly
412 (NEB E2621) or Quick Ligase (NEB M2200S). Restriction digests of backbone plasmids were
413 assembled with or ligated to GenScript gene fragments or polymerase chain reaction (PCR)
414 amplicons. Plasmids were purified from Stellar Competent *Escherichia coli* (Takara 636763)
415 using Azenta's standard plasmid prep service or using PureYield Plasmid Miniprep kit (Promega
416 A1223).

417

418 **Cell culture**

419 HEK293T cells (American Type Culture Collection (ATCC), CRL-3216), Neuro-2A cells
420 (ATCC, CCL-131), and MEF cells were grown in DMEM plus GlutaMAX (Gibco 10566-016)
421 supplemented with 10% (v/v) FBS (Gibco A56707-1) and 5% (v/v) Anti-Anti (Gibco 15240-062)
422 at 37°C with 5% CO_2 unless otherwise stated.

423 MEF cells were isolated from humanized *RBM20*^{R634Q} mutant homozygous mouse embryo
424 harvested at E13-E15. Embryo was covered in DPBS (Gibco 14190-144), and placenta and
425 maternal tissue were removed. Top of head was cut away and innards removed. Head was
426 retained for DNA isolation for genotyping. Embryo body was placed in 10cm plate (Corning
427 430167), 5mL 5x trypsin was added, and embryo was minced with razor blade and incubated at
428 37°C for 30-45 min. Trypsin activity was quenched with 5mL MEF media (DMEM with 10%
429 (v/v) FBS and 5% (v/v) Pen Strep (Gibco 15140-122)), and tissue was broken up by pipetting
430 10-20x. Sample was centrifuged, resuspended in 10mL MEF media, plated in 10cm plate, and
431 allowed to grow to confluency (3-4 days).

432

433 **Transfections of HEK293T, Neuro-2a, and MEF Cells**

434 Twenty-four hours before transfection, HEK293T and Neuro-2a cells at more than 90% viability
435 were seeded on 96-well plates (Thermo Fisher Scientific FB012931) at a density of 10,000-
436 12,000 cells per well. HEK293Ts were transfected with 0.3 µl of Lipofectamine 3000 (Thermo
437 Fisher Scientific L3000001) and 0.2 µl of P3000 with 100 ng of DNA in DMEM plus
438 GlutaMAX supplemented with 2% (v/v) FBS and 5% (v/v) Anti-Anti. Neuro-2a cells were
439 transfected with 0.35 µl Lipofectamine 2000 (Thermo Fisher Scientific 11668030) and 350 ng
440 DNA. HEK293T and Neuro-2a cells were co-transfected with dual PE cassette plasmids and two

441 linear DNA fragments encoding the ngRNA and pegRNA. Linear DNA fragments were
442 amplified from plasmid or from GenScript gene fragments using Q5 Hot Start High-Fidelity 2X
443 Master Mix (NEB M0494S) and primers [ACTCCATCACTAGGGGTTCCTG] and
444 [TTGGGAAGACAATAGCAGGCATG]. PCR reactions were performed with the following
445 conditions: 98°C 30 s; 12-18 cycles 98°C 10s, 67°C 20s, 72°C 20 sec; 72°C 2 min and purified
446 using QIAquick PCR Purification Kit (Qiagen 28106).

447 For HEK293T cell transfections, DNA was delivered in a 1:5 plasmid:linear DNA ratio, and for
448 Neuro-2a cell transfections, DNA was delivered in a 1:10 plasmid:linear DNA ratio. For each
449 replicate, 5 wells total were transfected (to be pooled after harvest) to average out potential well-
450 by-well discrepancies in cell density. 72 hours post-transfection, media was removed and cells
451 were harvested by adding 50 µl extraction buffer (Extraction Buffer (Abcam ab193970) +
452 Extraction Enhancer (Abcam ab193971) + cOmplete Protease Inhibitor Cocktail (Roche
453 11697498001)) per well and pipetting up and down.

454 For MEF transfections, ~80,000 cells per well were plated on 24-well plates (Corning 353047)
455 24 hours before transfection. MEFs were transfected at 80% confluency with 0.5 µl GenJet
456 (SignaGen Laboratories SL100489-MEF), 500 ng DNA, and 0.5 µl CombiMag (Oz Biosciences
457 CM20100) per well. DNA supplied was a single plasmid containing whole PE and both ngRNA
458 and pegRNA. For each replicate, two wells total were transfected (to be pooled after harvest).
459 After adding transfection mix, each plate was incubated on a magnetic plate (Oz Biosciences
460 MF10000) for 20 min at 37°C. Wells were replaced with fresh media 24 hours post-transfection.
461 72 hours post-transfection, cells were detached using TrypLE Express (Gibco 12604-013),
462 centrifuged at 300g for 5 min, and resuspended in 50 µl of extraction buffer.

463 For all cell lines, after harvest and pooling, samples were treated with proteinase K (Thermo
464 Scientific EO0491) at 55°C for 16 h, followed by 95°C for 20 min. The resulting lysates served
465 as gDNA templates in NGS editing efficiency analysis.

466

467 **gRNA selection**

468 For selection of optimized pegRNAs and ngRNAs targeting mouse *Rbm20*, several rounds of
469 screening were performed in Neuro-2a cells. For selection of optimized pegRNAs and ngRNAs
470 targeting human *RBM20*, several rounds of screening were performed in HEK293T cells with
471 validation of several tops hits in MEF cells from humanized $RBM20^{R636Q}$ mice. Variables
472 modified for the pegRNA include nick-site, RTT and PBS lengths, spacer length, post-edit DNA
473 sequence, and linker sequence. For the ngRNA, variables modified include nick-site and spacer
474 length. Various combinations of pegRNAs and ngRNAs were tested. Transfections and
475 harvesting were performed as described above.

476

477 **Recombinant AAV production**

478 We follow the standard HEK293T triple-transfection rAAV production and iodixanol gradient
479 ultracentrifugation purification protocol. Briefly, HEK293T cells were seeded to Corning
480 HYPERFlask Cell Culture Vessels at 50M cells per HYPERFlask in DMEM (Gibco, 10566024)
481 + 10% FBS (Gibco, 26140-095) + Antibiotic-Antimycotic (Gibco, 15240062). At ~48 hours post
482 seeding, 500 ug of DNA and 1 mg of PEI-MAX (Transporter 5 Transfection Reagent, Kyfora
483 Bio, 26008-50) were mixed and transfected to the cells in DMEM + 2% FBS + Antibiotic-
484 Antimycotic. For transfection DNA, 500 ug of pAdHelper + REP-CAP plasmid + transgene

485 cassette plasmid (1:1:1 molar ratio) were used. At ~72 hours post transfection, cells were
486 harvested by mechanical shaking, pelleted by spinning, resuspended in 150mM NaCl, 50mM
487 Tris-HCl, pH 8.5, and lysed by 4 freeze-thaw cycles. Next, non-encapsulated DNA in the lysate
488 was removed by 1 hour of Benzonase (Millipore, E1014) digestion at 37°C. After a 20-minute
489 centrifugation at 24,000 rcf, the supernatant was loaded to the top of an iodixanol gradient with
490 15%, 25%, 40%, and 60% layers. Following 1.5 hours of ultracentrifugation (Beckman Coulter
491 Type 70 Ti rotor, 59,000 rpm), 40% layer near the 40%-60% interface was extracted by a 5mL
492 sterile syringe attached to an 18-G needle. The extracted solution was desalted by Amicon®
493 Ultra-15 100kDa centrifugal filter (Millipore, PFHYS1008) in HBSS + 0.001% Pluronic F68
494 (Gibco, 24040-032) and the purified rAAV viruses were titered by Quant-iT PicoGreen dsDNA
495 assay (Invitrogen) following manufacturer's instructions.

496

497 **Mouse studies**

498 Animal studies were performed according to Tenaya Therapeutics' animal use guidelines. The
499 animal protocols were approved by the Institutional Animal Care and Use Committee (IACUC
500 number: 2023.007). All mice enrolled had C57BL/6 genetic background. *Rbm20*^{R636Q} knock-in
501 mice were obtained from University of Texas Southwestern Medical Center, and the information
502 on how they generated the mice was detailed in their publication. Cyagen Biomodels LLC (Santa
503 Clara, CA) was contracted for generating humanized RBM20 WT and R634Q mutant knock-in
504 mice utilizing CRISPR/Cas 9 system on C57BL/6N background. 2 male founders and 3 female
505 founders were obtained for each line initially, humanized knock-in sequences in the F1
506 generation were confirmed by sequencing. Both male and female mice were enrolled in all
507 studies. Ear tissue genomic DNA was extracted and used for genotyping.

508

509 **Echocardiography**

510 Cardiac function was assessed by transthoracic echocardiography using high resolution micro-
511 imaging systems (Vevo 3100 Preclinical Imaging System, VisualSonics). Briefly, anesthetized
512 spontaneously breathing mice (1-3% isoflurane and 98.5-99% O2) were placed in the supine
513 position on a temperature-controlled heating platform to maintain their body temperature at
514 ~37°C. Nair was used to remove hair and expose the skin to the probe. Parasternal short-axis M-
515 mode tracings of left ventricle (LV) were recorded for LV ejection fraction (EF) and LV internal
516 diameter in end systole and end diastole (LVID;s and LVID; d) calculation. Vevo Lab software
517 was used for analyses.

518

519 **Electrocardiogram recordings**

520 Mice were anesthetized with 1-1.5% isoflurane and 98.5-99% O2 via a nose cone (following
521 induction in a chamber containing 3-4% isoflurane in oxygen). Body temperature was monitored
522 continuously and maintained at 37–38 °C using a heat pad. Two lead ECG (leads II) were
523 recorded from sterile electrode needles (29-gauge) inserted subcutaneously into the right upper
524 chest with the negative electrode needle and into the left bottom chest with the positive electrode
525 needle. The signal was then acquired and analyzed using a digital acquisition and analysis
526 system (Power Lab; AD Instruments; LabChart 8 Pro software version). ECG parameters (QT
527 interval) were quantified after 1–2 min from the stabilized trace.

528

529 **Histology**

530 Mouse hearts were dissected, rinsed briefly in saline, and fixed overnight in 10% neutral
531 buffered formalin. Following fixation, tissues were dehydrated in 70% ethanol, and submitted to
532 HistoWiz Inc. (Long Island City NY) for sectioning and staining using a standardized automated
533 workflow. Serial transverse sections (5µm) were stained with hematoxylin and eosin (H&E) or
534 Masson's trichrome. Whole-slide scanning (40×) was performed on an Aperio AT2 (Leica
535 Biosystems).

536

537 ***Ex vivo* tissue processing**

538 Mice were anesthetized with 3-4% isoflurane and euthanized via cervical dislocation, followed
539 by heart and/or liver tissue collection. Whole hearts were harvested and cut to small pieces. Per
540 liver, one piece was taken from the left median lobe. Tissue was placed in 1.5 mL tubes
541 containing metal beads (Next Advance Inc., NAVYR1RNA) and flash-frozen in liquid nitrogen.
542 Tissue homogenization was performed using Precellys Evolution Touch Homogenizer (Bertin
543 Technologies P002511-PEVT0-A.0) with 5 cycles of 20 s 6500 rpm shaking and 10 s pause.

544 For DNA and RNA extraction from the same heart sample, tissue was homogenized in QIAzol
545 Lysis Reagent (Qiagen 79306) and processed using Direct-zol DNA/RNA Miniprep kit (Zymo
546 R2080). For DNA extraction only, heart tissue was homogenized in extraction buffer (Extraction
547 Buffer (Abcam ab193970) + Extraction Enhancer (Abcam ab193971) + cOmplete Protease
548 Inhibitor Cocktail (Roche 11697498001)) and digested with proteinase K (Thermo Scientific
549 EO0491) at 55°C for 16 h, followed by 95°C for 20 min, and gDNA was amplified directly from
550 lysate.

551 Heart RNA was treated with TURBO DNase (Thermo Fisher Scientific AM2238) at 37°C for 45
552 min then purified with *Quick*-RNA Miniprep kit (Zymo R1054). Treated RNA was reverse
553 transcribed using SuperScript IV First-Strand Synthesis System (Thermo Fisher Scientific
554 18091050) with random hexamers.

555 Liver tissue was processed using Quick-DNA Miniprep Plus Kit (Zymo D4068). Protocol was
556 altered slightly to include a homogenization step after addition of 400 µl Zymo kit lysis buffer
557 (solid tissues buffer and water) to tissue. After homogenization, samples were digested with
558 proteinase K for 1 hr at 55°C (1000 rpm shaking) and then centrifuged at 6000 g for 30 s.
559 Extraction was continued according to manufacturer's protocol using 200 µl supernatant.

560

561 **Quantitative real-time PCR analysis.**

562 qPCR reactions for splicing-related genes (*Ttn* and *Camk2d*) and for transgene (PE-N and PE-C
563 cassettes) were performed using PowerUp SYBR Green Master Mix (Applied Biosystems) on a
564 QuantStudio 7 Real-Time PCR System (Applied Biosystems). Primer sequences were as follows:
565 *Ttn N2B* forward: [GGAGTACACCTGCAAAGCCT], reverse:
566 [TGCGGCTTAGGTTCAGGAAG]; *Ttn N2BA* forward: [GGAGTACACCTGCAAAGCCT],
567 reverse: [CCTTGGGCCTGGAGAGAAAG] *Camk2d-A* forward:
568 [GCTCTACTGTTGCCTCCATG], reverse: [GCTGGTTACCACGTTGGC]; *Camk2d-B* forward:
569 [GTCCAGTTCGAGTGTTCAGA], reverse: [GCAGTGAGGCCTGGATCAC]; *Camk2d-C*
570 forward: [GCAGATGGGGTAAAGGAGT], reverse: [GGCAGTGAGGCCTGGATCAC]; PE-N
571 forward: [CGGATCTGCTATCTGCAAGAGATC], reverse:

572 [CTCGTGCTTCTTATCCTCTTCCAC]; PE-C forward:

573 [TGGTGGTGGCCAAAGTGGAAAAG], reverse: [AGTCGATGGGATTCTTCTCGAAGC].

574 For heart failure and cardiac fibrosis-related genes, qPCR was performed using TaqMan Fast

575 Advanced Master Mix (Applied Biosystems) with the following TaqMan Gene Expression

576 Assays: *Gapdh* (Mm99999915_g1); *Nppa* (Mm01255747_g1); *Nppb* (Mm01255770_g1); *Tgfb1*

577 (Mm01178820_m1); *Tgfb2* (Mm00436955_m1); *Col1a1* (Mm00801666_g1); *Col3a1*

578 (Mm00802300_m1)

579 Gene expression levels were normalized to *Gapdh* and reported as fold-change relative to the

580 control group.

581

582 **Next-generation sequencing and data analysis**

583 Genomic loci of interest were amplified from gRNA or cDNA via two rounds of PCR with

584 CloneAmp HiFi PCR Premix (Takara 639298). The initial PCR step was done using primers to

585 amplify the genomic locus and incorporate the primer binding site for the second round of PCR.

586 PCR reactions were amplified with the following conditions: 98°C for 30 s; n cycles of 98°C for

587 10 s, 60°C for 5 s and 72°C for 30 s (n = 16 when amplifying cDNA; n = 21-25 when amplifying

588 gDNA). The following primer pairs were used in the initial PCR step to amplify the specified

589 loci:

590 Mouse *Rbm20* editing site gDNA:

591 [tcgtcggcagcgtcagatgtgtataagagacagTCTCTTCCCTTCCTCCCAGGTATG] and

592 [gtctcgtgggctcggagatgtgtataagagacagTGTGCCCAAACATCCAACCTGTC]

593 Humanized mouse *RBM20* DNA editing site gDNA:

594 [tcgtcggcagcgtcagatgtgtataagagacagCTCCTTGGCTCCCTCACAGATATG] and

595 [gtctcgtgggctcggagatgtgtataagagacagTGTGCCCAAACATCCAACCTGTC]

596 Mouse *Rbm20* and humanized mouse *RBM20* editing site cDNA:

597 [tcgtcggcagcgtcagatgtgtataagagacagGACATGCTCCGGGAAGCTGAC] and

598 [gtctcgtgggctcggagatgtgtataagagacagTGTGCCCAAACATCCAACCTGTC]

599 Human *RBM20* editing site gDNA:

600 [tcgtcggcagcgtcagatgtgtataagagacagCTCCTTGGCTCCCTCACAGATATG] and

601 [gtctcgtgggctcggagatgtgtataagagacagTCCTGGCATAGGGAGAGTGCTC]

602 Human *RNF2* editing site gDNA:

603 [tcgtcggcagcgtcagatgtgtataagagacagAGGCTGTGCAGACAAACGGAAC] and

604 [gtctcgtgggctcggagatgtgtataagagacagCCAACATACAGAAGTCAGGAATGC]

605 Mouse *Dnmt1* editing site gDNA:

606 [tcgtcggcagcgtcagatgtgtataagagacagGGAGGCAAGCGCAGGCACTC] and

607 [gtctcgtgggctcggagatgtgtataagagacagTTGCCCTGTGTGGTACATGCTGC]

608 Mouse PE self-inactivation site:

609 [tcgtcggcagcgtcagatgtgtataagagacagAGACGCCTCCAGGCCACCATG] and

610 [gtctcgtgggctcggagatgtgtataagagacagTTCTTGCTGGGCACCTTGTACTC]

611 Unique Illumina index 1 and index 2 adapters were incorporated during the second PCR step by

612 amplifying first-round PCR product with Illumina DNA/RNA UD Indexes (Illumina 20091646,

613 20091647, 20061648, and 20061649). PCR reactions were amplified with the following cycle

614 conditions: 98°C for 30 s; 9 cycles of 98°C for 10 s, 55°C for 5 s, and 72°C for 30 s. Second-

615 round PCR product was size-selected and purified using E-Gel SizeSelect II Agarose Gels, 2%
616 (Invitrogen G661012). Purified libraries were quantified using Qubit dsDNA HS assay kit
617 (Thermo Fisher Q33231) and pooled for sequencing on Illumina NextSeq 550 using either the
618 NextSeq 500/550 High Output Reagent v2.5 75 cycles kit (20024906) or 150 cycles kit
619 (20024907), or, for sequencing of *in vitro* libraries, using the NextSeq 500/550 Mid Output v2.5
620 150 cycles kit (20024904).

621 Sequencing reads were de-multiplexed through Illumina's BaseSpace Sequence Hub. Sequence
622 extraction, unique sequence counting, and editing analysis were performed using an in-house
623 Python workflow. Briefly, a sequence of 36bp covering the editing site was extracted from NGS
624 reads with Q score > 30 (or > 20 for *in vitro* samples) at all positions in the extracted region.
625 Then, unique sequences were counted and sequence counts of each test sample were compared
626 against that of a control to generate a list of sequences occurring in the test sample either above a
627 frequency of 0.01 or enriched 3-fold above that sequence in the control and occurring in the test
628 sample above a frequency of 3 in a million (1 in ten thousands for *in vitro* samples). This step
629 removes most sequence variants generated by PCR errors and NGS errors. Finally, the frequency
630 of various PE outcomes (i.e. WT sequence, mutant sequence, fully edited sequence, partially
631 edited sequences, mutations and indels) were calculated from that list.

632

633 **Statistical analysis**

634 All data are shown as mean ± SD, mean ± SEM, mean ± SD with individual values from
635 biological replicates, or mean ± SEM with individual values from biological replicates as

indicated in the figure legends. Statistical analyses were performed with GraphPad Prism software. Statistical methods are indicated in the figure legends.

List of Supplementary Materials

Fig. S1 to S6

References and Notes

1. S. S. Martin, A. W. Aday, N. B. Allen, Z. I. Almarzooq, C. A. M. Anderson, P. Arora, C. L. Avery, C. M. Baker-Smith, N. Bansal, A. Z. Beaton, Y. Commodore-Mensah, M. E. Currie, M. S. V. Elkind, W. Fan, G. Generoso, B. B. Gibbs, D. G. Heard, S. Hiremath, M. C. Johansen, D. S. Kazi, D. Ko, M. H. Leppert, J. W. Magnani, E. D. Michos, M. E. Mussolino, N. I. Parikh, S. M. Perman, M. Rezk-Hanna, G. A. Roth, N. S. Shah, M. V. Springer, M.-P. St-Onge, E. L. Thacker, S. M. Urbut, H. G. C. Van Spall, J. H. Voeks, S. P. Whelton, N. D. Wong, S. S. Wong, K. Yaffe, L. P. Palaniappan, 2025 Heart Disease and Stroke Statistics: A Report of US and Global Data From the American Heart Association. *Circulation* **151**, e41–e660 (2025).

2. E. Jordan, L. Peterson, T. Ai, B. Asatryan, L. Bronicki, E. Brown, R. Celeghin, M. Edwards, J. Fan, J. Ingles, C. A. James, O. Jarinova, R. Johnson, D. P. Judge, N. Lahrouchi, R. H. Lekanne Deprez, R. T. Lumbers, F. Mazzarotto, A. Medeiros Domingo, R. L. Miller, A. Morales, B. Murray, S. Peters, K. Pilichou, A. Protonotarios, C. Semsarian, P. Shah, P. Syrris, C. Thaxton, J. P. Van Tintelen, R. Walsh, J. Wang, J. Ware,

657 R. E. Hershberger, Evidence-Based Assessment of Genes in Dilated Cardiomyopathy.
658 *Circulation* **144**, 7–19 (2021).

659 3. T. Nishiyama, Y. Zhang, M. Cui, H. Li, E. Sanchez-Ortiz, J. R. McAnally, W. Tan, J.
660 Kim, K. Chen, L. Xu, R. Bassel-Duby, E. N. Olson, Precise genomic editing of pathogenic
661 mutations in RBM20 rescues dilated cardiomyopathy. *Sci. Transl. Med.* **14**, eade1633
662 (2022).

663 4. M. Grosch, L. Schraft, A. Chan, L. Küchenhoff, K. Rapti, A.-M. Ferreira, J. Kornienko,
664 S. Li, M. H. Radke, C. Krämer, S. Clauder-Münster, E. Perlas, J. Backs, M. Gotthardt, C.
665 Dieterich, M. M. G. van den Hoogenhof, D. Grimm, L. M. Steinmetz, Striated muscle-
666 specific base editing enables correction of mutations causing dilated cardiomyopathy. *Nat.*
667 *Commun.* **14**, 3714 (2023).

668 5. A. C. Chai, M. Cui, F. Chemello, H. Li, K. Chen, W. Tan, A. Atmanli, J. R. McAnally,
669 Y. Zhang, L. Xu, N. Liu, R. Bassel-Duby, E. N. Olson, Base editing correction of
670 hypertrophic cardiomyopathy in human cardiomyocytes and humanized mice. *Nat. Med.*
671 **29**, 401–411 (2023).

672 6. D. Reichart, G. A. Newby, H. Wakimoto, M. Lun, J. M. Gorham, J. J. Curran, A.
673 Raguram, D. M. DeLaughter, D. A. Conner, J. D. C. Marsiglia, S. Kohli, L. Chmatal, D.
674 C. Page, N. Zabaleta, L. Vandenberghe, D. R. Liu, J. G. Seidman, C. Seidman, Efficient in
675 vivo genome editing prevents hypertrophic cardiomyopathy in mice. *Nat. Med.* **29**, 412–
676 421 (2023).

677 7. L. Yang, Z. Liu, J. Sun, Z. Chen, F. Gao, Y. Guo, Adenine base editor-based correction
678 of the cardiac pathogenic Lmna c. 1621C > T mutation in murine hearts. *J. Cell. Mol.*
679 *Med.* **28**, e18145 (2024).

680 8. S. Lebek, X. M. Caravia, L. G. Straub, D. Alzhanov, W. Tan, H. Li, J. R. McAnally, K.
681 Chen, L. Xu, P. E. Scherer, N. Liu, R. Bassel-Duby, E. N. Olson, CRISPR-Cas9 base
682 editing of pathogenic CaMKIIδ improves cardiac function in a humanized mouse model.
683 *Journal of Clinical Investigation* **134**, e175164 (2024).

684 9. S. Ma, W. Jiang, X. Liu, W. J. Lu, T. Qi, J. Wei, F. Wu, Y. Chang, S. Zhang, Y. Song, R.
685 Bai, J. Wang, A. S. Lee, H. Zhang, Y. Wang, F. Lan, Efficient Correction of a Hypertrophic
686 Cardiomyopathy Mutation by ABEmax-NG. *Circ. Res.* **129**, 895–908 (2021).

687 10. A. Roman, A. Zimmer, M. Gotthardt, L. M. Steinmetz, R. Kühn, T. Dang, Prime
688 editing corrects the dilated cardiomyopathy causing RBM20-P633L-mutation in human
689 cardiomyocytes. *Mol. Ther. Nucleic Acids* **36**, 102734 (2025).

690 11. A. V. Anzalone, P. B. Randolph, J. R. Davis, A. A. Sousa, L. W. Koblan, J. M. Levy, P.
691 J. Chen, C. Wilson, G. A. Newby, A. Raguram, D. R. Liu, Search-and-replace genome
692 editing without double-strand breaks or donor DNA. *Nature* **576**, 149–157 (2019).

693 12. T. Nishiyama, Prime Editing Corrects Multiple Mutations in the RSRSP Region of the
694 RBM20 Gene Using a Single Prime Editing Guide RNA. *JMA J.* **8**, 587–590 (2025).

695 13. K. She, Y. Liu, Q. Zhao, X. Jin, Y. Yang, J. Su, R. Li, L. Song, J. Xiao, S. Yao, F. Lu,
696 Y. Wei, Y. Yang, Dual-AAV split prime editor corrects the mutation and phenotype in mice
697 with inherited retinal degeneration. *Signal Transduct. Target. Ther.* **8**, 57 (2023).

14. S. Zhi, Y. Chen, G. Wu, J. Wen, J. Wu, Q. Liu, Y. Li, R. Kang, S. Hu, J. Wang, P. Liang, J. Huang, Dual-AAV delivering split prime editor system for in vivo genome editing. *Molecular Therapy* **30**, 283–294 (2022).

15. J. R. Davis, S. Banskota, J. M. Levy, G. A. Newby, X. Wang, A. V Anzalone, A. T. Nelson, P. J. Chen, A. D. Hennes, M. An, H. Roh, P. B. Randolph, K. Musunuru, D. R. Liu, Efficient prime editing in mouse brain, liver and heart with dual AAVs. *Nat. Biotechnol.* **42**, 253–264 (2024).

16. D. L. Brooks, M. N. Whittaker, P. Qu, K. Musunuru, R. C. Ahrens-Nicklas, X. Wang, Efficient in vivo prime editing corrects the most frequent phenylketonuria variant, associated with high unmet medical need. *The American Journal of Human Genetics* **110**, 2003–2014 (2023).

17. R. Wei, Z. Yu, L. Ding, Z. Lu, K. Yao, H. Zhang, B. Huang, M. He, L. Ma, Improved split prime editors enable efficient in vivo genome editing. *Cell Rep.* **44**, 115144 (2025).

18. A. A. Sousa, M. Terrey, H. A. Sakai, C. Q. Simmons, E. Arystarkhova, N. S. Morsci, L. C. Anderson, J. Xie, F. Suri-Payer, L. C. Laux, E. Roze, S. Forlani, G. Gao, S. Frost, N. Frost, K. J. Sweadner, A. L. George, C. M. Lutz, D. R. Liu, In vivo prime editing rescues alternating hemiplegia of childhood in mice. *Cell* **188**, 4275-4294.e23 (2025).

19. Y. Fu, X. He, L. Ma, X. D. Gao, P. Liu, H. Shi, P. Chai, S. Ge, R. Jia, D. R. Liu, X. Fan, Z. Yang, In vivo prime editing rescues photoreceptor degeneration in nonsense mutant retinitis pigmentosa. *Nat. Commun.* **16**, 2394 (2025).

718 20. Z. Gao, S. Ravendran, N. S. Mikkelsen, J. Haldrup, H. Cai, X. Ding, S. R. Paludan, M.
719 K. Thomsen, J. G. Mikkelsen, R. O. Bak, A truncated reverse transcriptase enhances prime
720 editing by split AAV vectors. *Molecular Therapy* **30**, 2942–2951 (2022).

721 21. J. Koelemen, M. Gotthardt, L. M. Steinmetz, B. Meder, RBM20-Related
722 Cardiomyopathy: Current Understanding and Future Options. *J. Clin. Med.* **10**, 4101
723 (2021).

724 22. T. M. Hey, T. B. Rasmussen, T. Madsen, M. M. Aagaard, M. Harbo, H. Mølgaard, J. E.
725 Møller, H. Eiskjær, J. Mogensen, Pathogenic RBM20 -Variants Are Associated With a
726 Severe Disease Expression in Male Patients With Dilated Cardiomyopathy. *Circ. Heart*
727 *Fail.* **12**, e005700 (2019).

728 23. A. Greer-Short, A. Greenwood, E. C. Leon, T. N. Qureshi, K. von Kraut, J. Wong, J.
729 H. Tsui, C. A. Reid, Z. Cheng, E. Easter, J. Yang, J. Ho, S. Steltzer, A. Budan, M. Cho, R.
730 Chandrakumar, O. Cisne-Thompson, C. Feathers, T. W. Chung, N. Rodriguez, S. Jones, C.
731 Alleyne-Levy, J. Liu, F. Jing, W. S. Prince, J. Lin, K. N. Ivey, W. G. Tingley, T. Hoey, L.
732 M. Lombardi, AAV9-mediated MYBPC3 gene therapy with optimized expression cassette
733 enhances cardiac function and survival in MYBPC3 cardiomyopathy models. *Nat.*
734 *Commun.* **16**, 2196 (2025).

735 24. J. Yan, P. Oyler-Castrillo, P. Ravisankar, C. C. Ward, S. Levesque, Y. Jing, D.
736 Simpson, A. Zhao, H. Li, W. Yan, L. Goudy, R. Schmidt, S. C. Solley, L. A. Gilbert, M. M.
737 Chan, D. E. Bauer, A. Marson, L. R. Parsons, B. Adamson, Improving prime editing with
738 an endogenous small RNA-binding protein. *Nature* **628**, 639–647 (2024).

25. M. M. G. van den Hoogenhof, A. Beqqali, A. S. Amin, I. van der Made, S. Aufiero, M. A. F. Khan, C. A. Schumacher, J. A. Jansweijer, K. Y. van Spaendonck-Zwarts, C. A. Remme, J. Backs, A. O. Verkerk, A. Baartscheer, Y. M. Pinto, E. E. Creemers, RBM20 Mutations Induce an Arrhythmogenic Dilated Cardiomyopathy Related to Disturbed Calcium Handling. *Circulation* **138**, 1330–1342 (2018).

26. J. L. Doman, S. Pandey, M. E. Neugebauer, M. An, J. R. Davis, P. B. Randolph, A. McElroy, X. D. Gao, A. Raguram, M. F. Richter, K. A. Everette, S. Banskota, K. Tian, Y. A. Tao, J. Tolar, M. J. Osborn, D. R. Liu, Phage-assisted evolution and protein engineering yield compact, efficient prime editors. *Cell* **186**, 3983–4002 (2023).

27. K. M. Brauch, M. L. Karst, K. J. Herron, M. de Andrade, P. A. Pellikka, R. J. Rodeheffer, V. V. Michels, T. M. Olson, Mutations in Ribonucleic Acid Binding Protein Gene Cause Familial Dilated Cardiomyopathy. *J. Am. Coll. Cardiol.* **54**, 930–941 (2009).

28. T. Lan, H. Chen, C. Tang, Y. Wei, Y. Liu, J. Zhou, Z. Zhuang, Q. Zhang, M. Chen, X. Zhou, Y. Chi, J. Wang, Y. He, L. Lai, Q. Zou, Mini-PE, a prime editor with compact Cas9 and truncated reverse transcriptase. *Mol. Ther. Nucleic Acids* **33**, 890–897 (2023).

29. B. J. Rauch, A. DeLoughery, R. Sper, S. Chen, S. Yunanda, M. Masnaghetti, N. Chai, J. C. Lin, A. Neckelmann, Y. Bjornson, D. P. Espino, A. Sancio, C. Schmitt, C. Scholes, R. Shah, P. K. Narendra, S. Ansaloni, S. Tan, S. J. Rukmini, S. Somaiah, S. Suresh, S. Minami, S. Tymoshenko, W. Wright, S. Xu, J. Broughton, M. D. Retwitzer, M. Bobbin, D. Yuan, K. Abe, M. DeWitt, B. Zhang, L. B. Harrington, Single-AAV CRISPR editing of skeletal muscle in non-human primates with NanoCas, an ultracompact nuclease**9**, 1–21 (2025).

30. J. Grünewald, B. R. Miller, R. N. Szalay, P. K. Cabeceiras, C. J. Woodilla, E. J. B. Holtz, K. Petri, J. K. Joung, Engineered CRISPR prime editors with compact, untethered reverse transcriptases. *Nat. Biotechnol.* **41**, 337–343 (2023).

31. L. Suarez-Amaran, L. Song, A. P. Tretiakova, S. A. Mikhail, R. J. Samulski, AAV vector development, back to the future. *Molecular Therapy* **33**, 1903–1936 (2025).

Acknowledgements: We thank Eric Olson and his laboratory for providing the *Rbm20*^{R636Q} mouse model. We thank the vivarium team at Tenaya Therapeutics for animal husbandry support.

Funding: not applicable.

Author contributions: W.L. generated the humanized *RBM20* mouse model and conducted *in vivo* experiments and *ex vivo* analyses. L.M.R. cloned PE constructs, manufactured AAV for *in vivo* experiments, and conducted *ex vivo* analyses. E.E. developed guide RNAs targeting human *RBM20*, cloned PE constructs, and manufactured AAV for *in vivo* experiments. H.Z. designed the humanized *RBM20* mouse model and performed MEF isolation. C.D.H. contributed to mouse genotyping and *in vivo* experiments. A.G.S., T.H., L.M.L., and K.N.I. supervised the research. Z.C. designed the studies and performed viral injections. W.L., L.M.R., and Z.C. prepared the manuscript with input from all authors.

Competing interests: W.L., L.M.R., E.E., H.Z., C.D.H., A.G.S., T.H., L.M.L., K.N.I., and Z.C. performed this research as part of their employment at Tenaya Therapeutics. W.L., L.M.R., E.E.,

781 H.Z., and Z.C. are inventors of patent applications filed by Tenaya Therapeutics relating to the
782 work described in this article.

783 **Data and materials availability:** All data supporting the findings described in this manuscript
784 are available in the article and in the Supplementary Materials. Sequences are available in the
785 Materials and Methods and Supplementary Materials.

786

Supplementary Materials

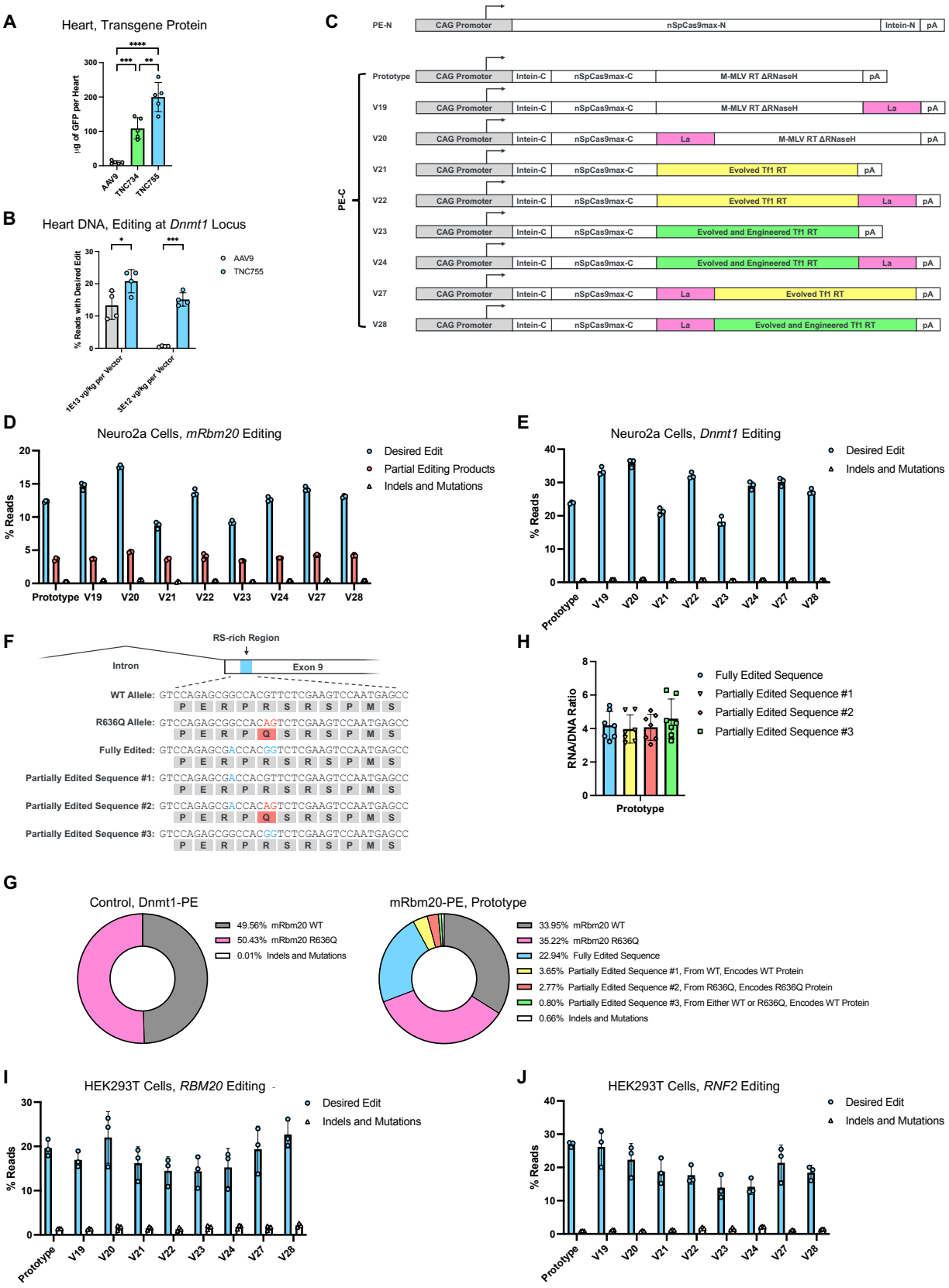
A
Heart, Transgene Protein
µg of GFP per Heart
AAV9
TNC734
TNC755
B
Heart DNA, Editing at Dnmt1 Locus
% Reads with Desired Edit
AAV9
TNC755
1E13 vg/kg per Vector
3E12 vg/kg per Vector
C
PE-N
CAG Promoter
nSpCas9max-N
Intein-N
pA
PE-C
Prototype
V19
V20
V21
V22
V23
V24
V27
V28
Intein-C
nSpCas9max-C
M-MLV RT ΔRNaseH
La
Evolved Tf1 RT
Evolved and Engineered Tf1 RT
D
Neuro2a Cells, mRbm20 Editing
% Reads
Desired Edit
Partial Editing Products
Indels and Mutations
E
Neuro2a Cells, Dnmt1 Editing
% Reads
Desired Edit
Indels and Mutations
F
RS-rich Region
Intron
Exon 9
WT Allele: GTCCAGAGCGGCCACGTTCTCGAAGTCCAATGAGCC
P E R P R S R S P M S
R636Q Allele: GTCCAGAGCGGCCACAGTCTCGAAGTCCAATGAGCC
P E R P Q S R S P M S
Fully Edited: GTCCAGAGCGACCACGGTCTCGAAGTCCAATGAGCC
P E R P R S R S P M S
Partially Edited Sequence #1: GTCCAGAGCGACCACGTTCTCGAAGTCCAATGAGCC
P E R P R S R S P M S
Partially Edited Sequence #2: GTCCAGAGCGACCACAGTCTCGAAGTCCAATGAGCC
P E R P Q S R S P M S
Partially Edited Sequence #3: GTCCAGAGCGGCCACGGTCTCGAAGTCCAATGAGCC
P E R P R S R S P M S
H
RNA/DNA Ratio
Prototype
Fully Edited Sequence
Partially Edited Sequence #1
Partially Edited Sequence #2
Partially Edited Sequence #3
G
Control, Dnmt1-PE
49.56% mRbm20 WT
50.43% mRbm20 R636Q
0.01% Indels and Mutations
mRbm20-PE, Prototype
33.95% mRbm20 WT
35.22% mRbm20 R636Q
22.94% Fully Edited Sequence
3.65% Partially Edited Sequence #1, From WT, Encodes WT Protein
2.77% Partially Edited Sequence #2, From R636Q, Encodes R636Q Protein
0.80% Partially Edited Sequence #3, From Either WT or R636Q, Encodes WT Protein
0.66% Indels and Mutations
I
HEK293T Cells, RBM20 Editing
% Reads
Desired Edit
Indels and Mutations
J
HEK293T Cells, RNF2 Editing
% Reads
Desired Edit
Indels and Mutations

789 **Fig. S1. Developing a dual-AAV based strategy for *in vivo* cardiac prime editing (PE).** (**A**) Expression levels of
790 EGFP transgene protein in the heart mediated by AAV9 and in-house engineered capsids. C57BL/6J mice at 6 weeks
791 of age were administered with either WT AAV9 or one of our in-house engineered capsids (sequences available
792 upon request) containing EGFP transgene under control of the 400bp *TNNT2*-derived promoter (1E13 vg/kg, 5
793 animals per group) via RO injection. Mice were euthanized 3 weeks post-injection and EGFP expression in the heart
794 was assessed using Abcam GFP ELISA kit (ab171581). (**B**) *In vivo* cardiac editing efficiencies and cardiac
795 transduction levels mediated by AAV9 and TNC755. TNC755 was used in efficacy studies described in this
796 manuscript. C57BL/6J mice were administered with either WT AAV9 or one of our engineered capsids containing
797 PE-N and PE-C cassettes targeting the *Dnmt1* locus (1E13 vg/kg or 3E12 vg/kg, 4 animals per group) via RO
798 injection. Mice were euthanized 3 weeks post-injection and DNA and RNA were isolated from whole heart. *Dnmt1*
799 editing efficiency was determined via NGS and transgene DNA transduction and RNA expression were quantified
800 via qPCR (normalized to GAPDH, average of PE-N and PE-C). For A and B, dots represent individual mice.
801 Statistical significance was calculated using one-way ANOVA with Tukey's multiple comparisons test. *$P < 0.05$,
802 **$P < 0.01$, ***$P < 0.001$, ****$P < 0.0001$. (**C**) Schematic of our PE cassettes for *in vitro* experiments. (**D** and **E**) *In*
803 *vitro* editing efficiency at the target locus of Neuro2a cells transfected with PE-N and PE-C cassettes and
804 pegRNA/ngRNA targeting either the mouse *Rbm20* (D) or *Dnmt1* (E) locus. (**F**) Schematic demonstrating possible
805 post-edit outcomes in *Rbm20*$^{R636Q/+}$ mice edited using our mRbm20-PE. (**G**) Mean percentages of *Rbm20* editing
806 outcomes in *Rbm20*$^{R636Q/+}$ mice treated with Dnmt1-PE (control) or mRbm20-PE prototype. (**H**) RNA/DNA ratio of
807 different post-edit sequences from mice treated with mRbm20-PE Prototype. Dots represent individual mice and
808 error bars represent mean ± SD. (**I** and **J**) *In vitro* editing efficiency at the target locus of HEK293T cells transfected
809 with PE-N and PE-C cassettes and pegRNA/ngRNA targeting either the *RBM20* (I) or *RNF2* (J) locus. For D, E, I,
810 and J, dots represent individual biological replicates, and error bars represent mean ± SD.

811

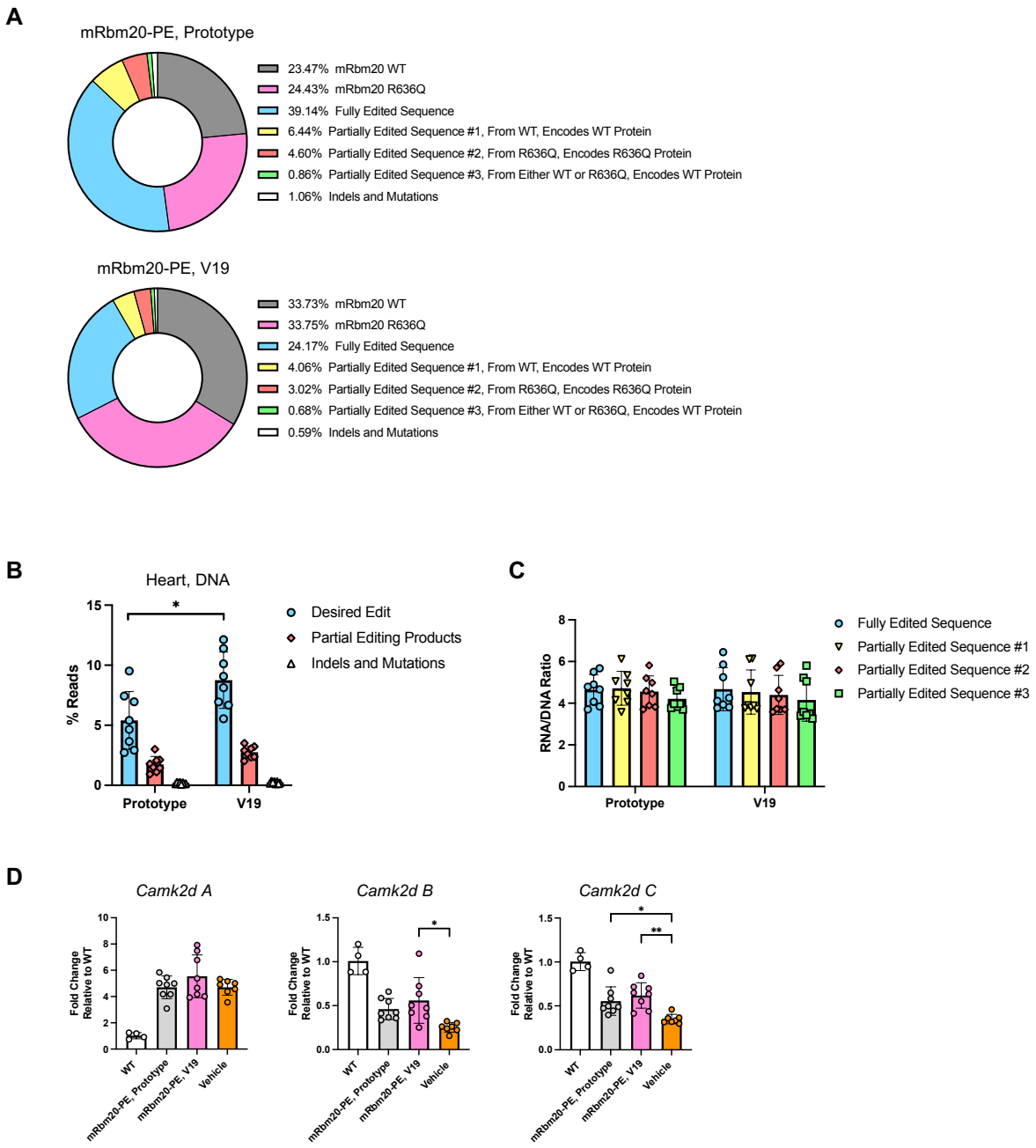

Fig. S2. V19 prime editor improves editing efficiency and rescues phenotypes in *Rbm20*^{R636Q} DCM mouse model. (**A**) Mean percentages of *Rbm20* editing outcomes in *Rbm20*$^{R636Q/+}$ mice treated with mRbm20-PE Prototype or mRbm20-PE V19 (4.6E13 vg/kg per vector). (**B**) Editing efficiency at the *Rbm20* locus, detected from whole heart DNA samples. (**C**) RNA/DNA ratio of different post-edit sequences. (**D**) Splicing patterns of *Camk2d* gene. For B to D, dots represent individual mice, error bars represent mean ± SD. For B, statistical significance was

818 calculated using unpaired t-test. For D, statistical significance was calculated using two-way ANOVA with Tukey's

819 multiple comparisons test. *$P < 0.05$, **$P < 0.01$.

820

A
mRbm20-PE, V19
53.22% mRbm20 WT
34.50% Fully Edited Sequence
10.77% Partially Edited Sequence #1, From WT, Encodes WT Protein
0.72% Partially Edited Sequence #3, From Either WT or R636Q, Encodes WT Protein
0.80% Indels and Mutations
mRbm20-PE, V20
8.34% mRbm20 WT
74.46% Fully Edited Sequence
15.00% Partially Edited Sequence #1, From WT, Encodes WT Protein
0.17% Partially Edited Sequence #3, From Either WT or R636Q, Encodes WT Protein
2.03% Indels and Mutations
mRbm20-PE, V22
37.15% mRbm20 WT
50.82% Fully Edited Sequence
10.15% Partially Edited Sequence #1, From WT, Encodes WT Protein
0.61% Partially Edited Sequence #3, From Either WT or R636Q, Encodes WT Protein
1.28% Indels and Mutations
mRbm20-PE, V24
12.91% mRbm20 WT
77.06% Fully Edited Sequence
8.06% Partially Edited Sequence #1, From WT, Encodes WT Protein
0.27% Partially Edited Sequence #3, From Either WT or R636Q, Encodes WT Protein
1.71% Indels and Mutations
B
SI Site
nSpCas9max-N
Intein-N
PE-N
PE
Intein-C
nSpCas9max-C
M-MLV RT ΔRNaseH
La
PE-C
PE
Target Genomic Locus
Mutations Corrected
SI Site
nSpCas9max-N
Intein-N
Amino Acid Change(s), Frameshift, and/or Premature Stop Codon(s)
C
Regular PE-N:
nSpCas9max-N
Intein-N
ATG AAA CGG ACA GCC GAC GGA AGC GAG ... ...
M K R T A D G S E
SI PE-N:
SI Site
nSpCas9max-N
Intein-N
ATG CCT CCC AGG TAT GGT CCA GAG CGG CCA CGC TCG AAG TCC AAT GAG CTA AAA CGG ACA GCC GAC GGA AGC GAG ...
M P P R Y G P E R P R S K S N E L K R T A D G S E
SI PE-N Post-SI:
SI Site
nSpCas9max-N
Intein-N
Amino Acid Change(s), Frameshift, and/or Premature Stop Codon(s)
+2 Insertion
ATG CCT CCC AGG TAT GGT CCA GAG CGa CCA CGg tCT CGA AGT CCA ATG AGC TAA AAC GGA CAG CCG ACG GAA GCG AG ...
M P P R Y G P E R P R S R S P M S X
D
PE-N
PE-C
4 Weeks of Age, RO Injection
2.8E13 vg/kg per Vector
8 Weeks Post-Injection
Ex Vivo Analysis
Heart, RNA
% Reads with Desired Edit
30
20
10
0
Editing at Rbm20 Locus
Editing at SI Site

821

822 **Fig. S3. Engineering prime editors to enhance editing efficiency and/or enable self-inactivation.** (**A**) Mean
823 percentages of *Rbm20* editing outcomes in mice treated with mRbm20-PE V19, V20, V22, and V24 (2.E13 vg/kg
824 per vector). WT mice were used in this study. (**B**) Schematic detailing our self-inactivation (SI) strategy: an SI site is
825 a polynucleotide sequence which encodes a short peptide and can be recognized and edited by the prime editor; the
826 SI site is incorporated to the coding region of PE-N and/or PE-C; the unedited SI site adds a short peptide to the PE
827 protein and the resulting fusion protein is still functional; once introduced to the cell, PE happens at both the
828 genomic target locus and the SI site; PE at the SI site introduces amino acid change(s), frameshift, and/or premature
829 stop codon(s); the post-editing SI site inactivates the expression and/or function of the PE protein. (**C**) Schematic of
830 a SI PE example, carrying an SI site that can be edited by our mouse *Rbm20*-targeting pegRNA. (**D**) *In vivo* cardiac
831 editing at *Rbm20* locus and SI site by mRBM20-SI-PE V19. *Ex vivo* analysis was performed at 8 weeks post-
832 injection. Dots represent individual mice, and error bars represent mean ± SD.

833

834

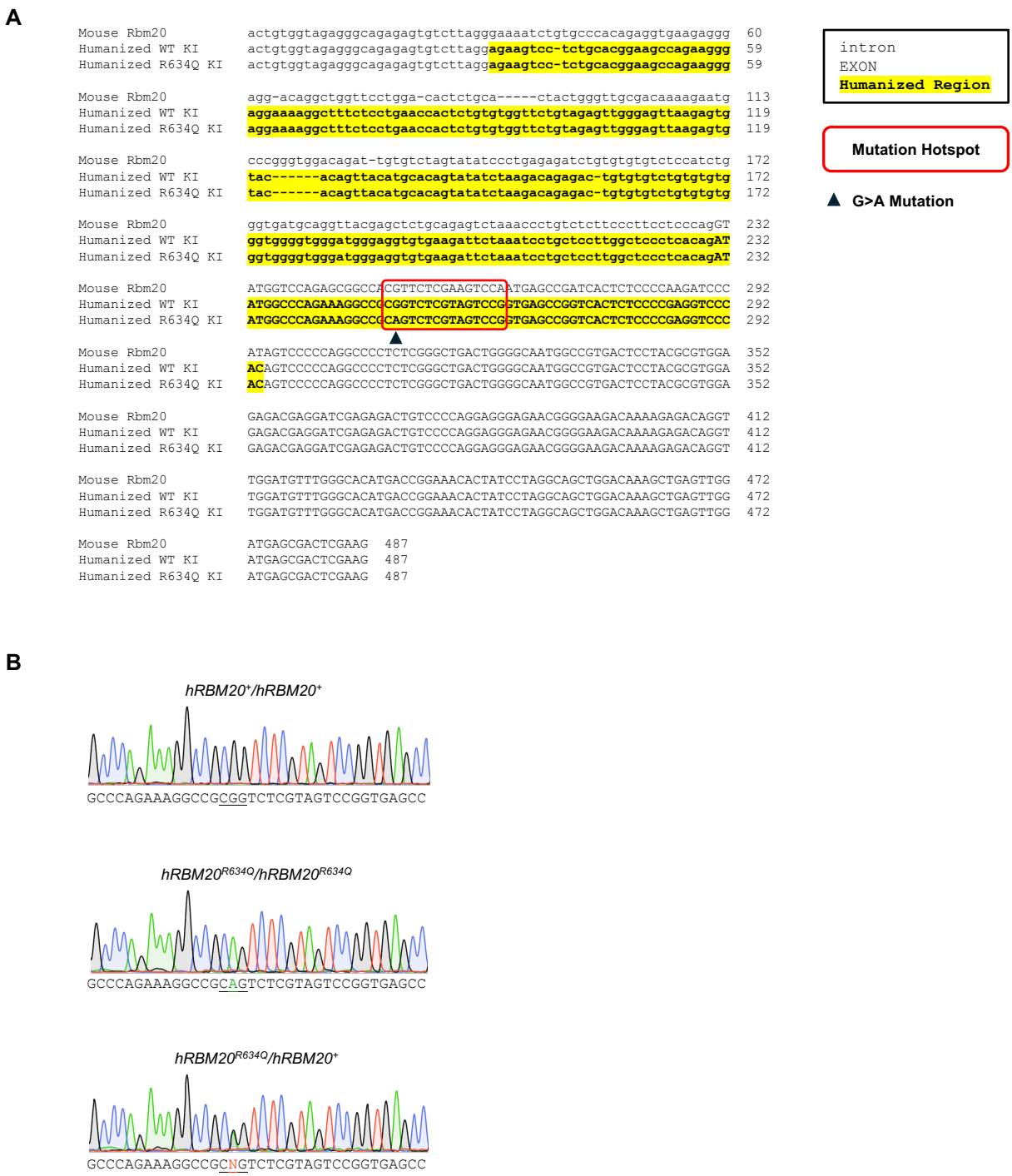

Fig. S4. Generating a novel humanized *RBM20* mouse model. (**A**) Sequence comparison of mouse *Rbm20*, human *RBM20*, and human *RBM20*^{R634Q} indicating intron and exon regions, humanized region, mutation hotspot, and R634Q G>A mutation. (**B**) Sanger sequencing confirmation of humanized mouse genotypes.

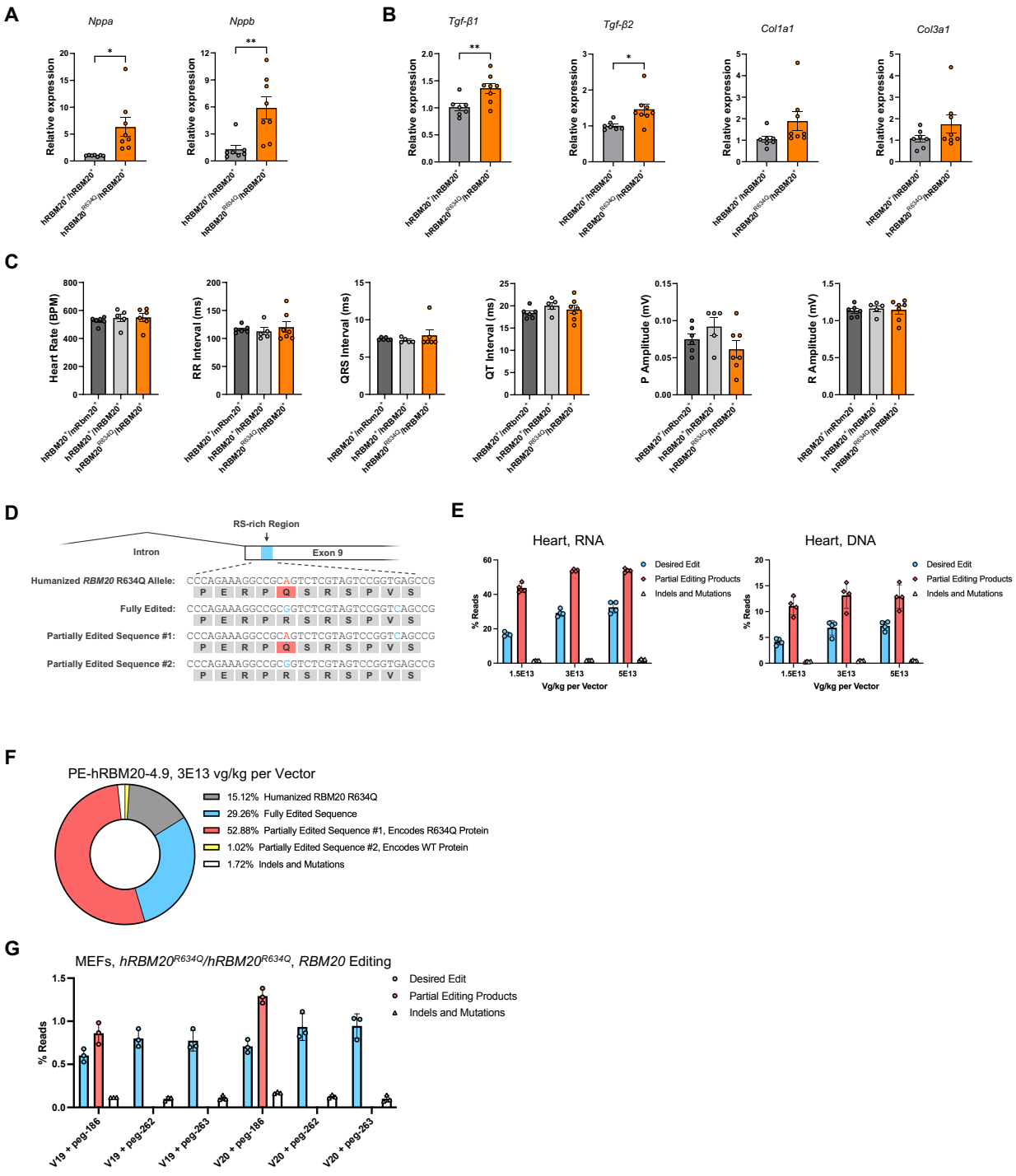

Fig. S5. Humanized *RBM20* mouse model exhibits *RBM20* cardiomyopathy phenotypes and facilitates the development of human *RBM20* PE. Quantitative PCR analysis of (**A**) heart failure markers *Nppa* and *Nppb* and (**B**) fibrosis-related genes in heterozygous mouse hearts. (**C**) Electrocardiogram analysis showed normal electrophysiological parameters in heterozygous mice. (**D**) Schematic demonstrating possible post-edit

845 outcomes for *hRBM20*^{R634Q} allele edited using PE-hRBM20-4.9. (**E**) *hRBM20*^{R634Q} editing outcomes in RNA or
846 DNA isolated from whole heart of *hRBM20*^{R634Q}*/mRBM20*$^{+}$ mice treated with PE-hRBM20-4.9 at 1.5E13, 3E13, or
847 5E13 vg/kg per vector. (**F**) Mean percentage of *RBM20* editing outcomes in RNA isolated from whole heart of
848 *hRBM20*^{R634Q}*/mRBM20*$^{+}$ mice treated with PE-hRBM20-4.9 at 3E13 vg/kg per vector. Dots represent individual
849 mice, error bars represent mean ± SD. **P* < 0.05, ***P* < 0.01. (**G**) *In vitro RBM20* editing efficiency of
850 *hRBM20*^{R634Q}*/hRBM20*^{R634Q} MEF cells transfected with *in vitro* V19 or V20 PE cassette containing h-ng-26 and one
851 of three pegRNAs. Dots represent biological replicates, error bars represent mean ± SD.

852

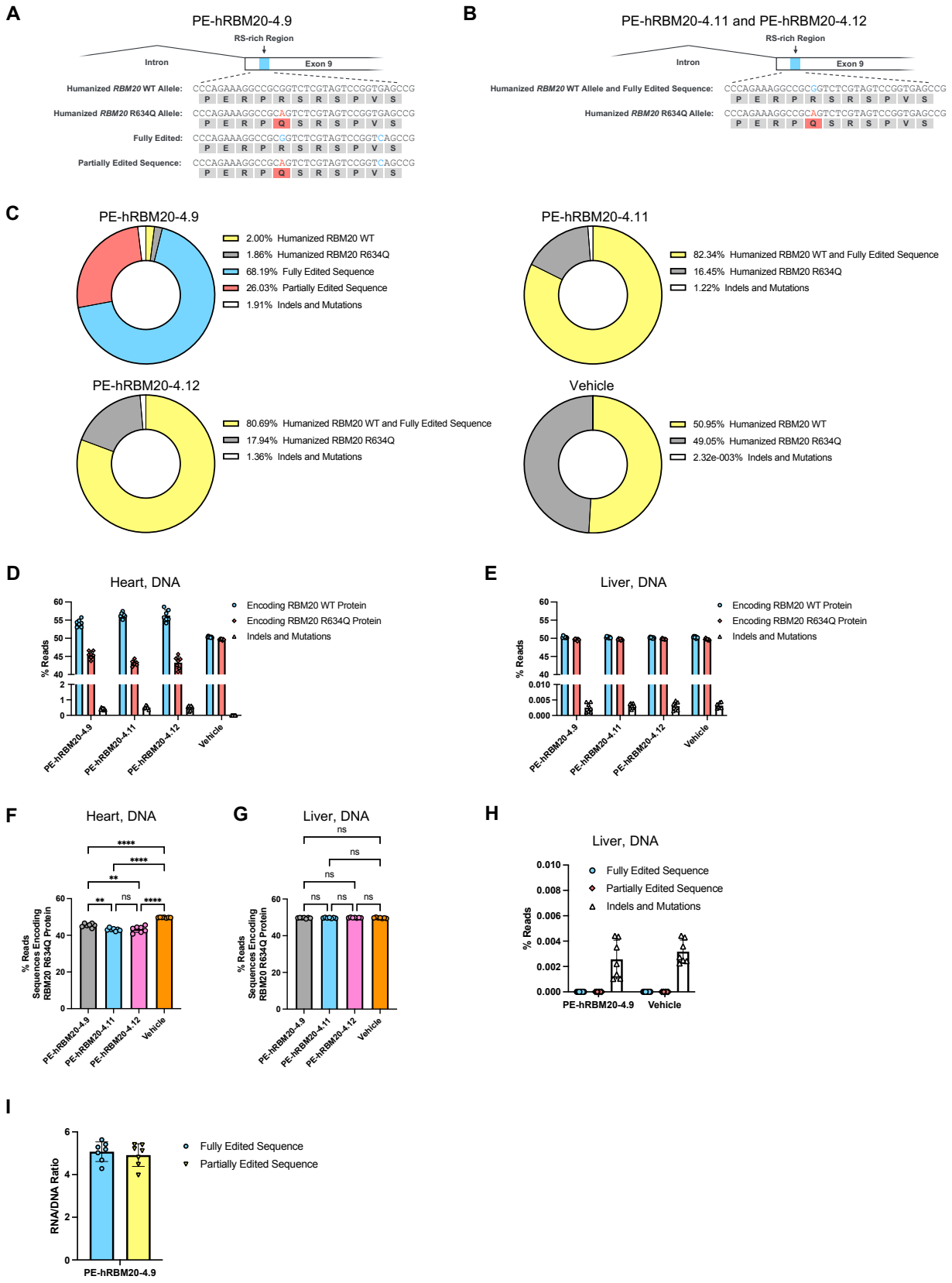
A
PE-hRBM20-4.9
RS-rich Region
Intron
Exon 9
Humanized RBM20 WT Allele: CCCAGAAAGGCCGCGGTCTCGTAGTCCGGTGAGCCG
P E R P R S R S P V S
Humanized RBM20 R634Q Allele: CCCAGAAAGGCCGCAGTCTCGTAGTCCGGTGAGCCG
P E R P Q S R S P V S
Fully Edited: CCCAGAAAGGCCGCGGTCTCGTAGTCCGGTCAGCCG
P E R P R S R S P V S
Partially Edited Sequence: CCCAGAAAGGCCGCAGTCTCGTAGTCCGGTCAGCCG
P E R P Q S R S P V S
B
PE-hRBM20-4.11 and PE-hRBM20-4.12
RS-rich Region
Intron
Exon 9
Humanized RBM20 WT Allele and Fully Edited Sequence: CCCAGAAAGGCCGCGGTCTCGTAGTCCGGTGAGCCG
P E R P R S R S P V S
Humanized RBM20 R634Q Allele: CCCAGAAAGGCCGCAGTCTCGTAGTCCGGTGAGCCG
P E R P Q S R S P V S
C
PE-hRBM20-4.9
2.00% Humanized RBM20 WT
1.86% Humanized RBM20 R634Q
68.19% Fully Edited Sequence
26.03% Partially Edited Sequence
1.91% Indels and Mutations
PE-hRBM20-4.11
82.34% Humanized RBM20 WT and Fully Edited Sequence
16.45% Humanized RBM20 R634Q
1.22% Indels and Mutations
PE-hRBM20-4.12
80.69% Humanized RBM20 WT and Fully Edited Sequence
17.94% Humanized RBM20 R634Q
1.36% Indels and Mutations
Vehicle
50.95% Humanized RBM20 WT
49.05% Humanized RBM20 R634Q
2.32e-003% Indels and Mutations
D
Heart, DNA
% Reads
Encoding RBM20 WT Protein
Encoding RBM20 R634Q Protein
Indels and Mutations
PE-hRBM20-4.9
PE-hRBM20-4.11
PE-hRBM20-4.12
Vehicle
E
Liver, DNA
% Reads
Encoding RBM20 WT Protein
Encoding RBM20 R634Q Protein
Indels and Mutations
PE-hRBM20-4.9
PE-hRBM20-4.11
PE-hRBM20-4.12
Vehicle
F
Heart, DNA
% Reads Sequences Encoding RBM20 R634Q Protein
PE-hRBM20-4.9
PE-hRBM20-4.11
PE-hRBM20-4.12
Vehicle
G
Liver, DNA
% Reads Sequences Encoding RBM20 R634Q Protein
PE-hRBM20-4.9
PE-hRBM20-4.11
PE-hRBM20-4.12
Vehicle
H
Liver, DNA
% Reads
Fully Edited Sequence
Partially Edited Sequence
Indels and Mutations
PE-hRBM20-4.9
Vehicle
I
RNA/DNA Ratio
Fully Edited Sequence
Partially Edited Sequence
PE-hRBM20-4.9

853

854 **Fig. S6. *In vivo* cardiac PE successfully corrects *RBM20*^{R634Q} in mouse heart without showing detectable**
855 **editing in off-target tissue.** (**A** and **B**) Schematic depicting editing outcomes of humanized *hRBM20*^{R634Q}*/hRBM20*$^{+}$
856 mice treated with PE-hRBM20-4.9 (A) or PE-hRBM20-4.11 and PE-hRBM20-4.12 (B). (**C**) Mean percentages of
857 *RBM20* editing outcomes in RNA of *hRBM20*^{R634Q}*/hRBM20*$^{+}$ mice treated with PE-hRBM20-4.9, PE-hRBM20-4.11,
858 PE-hRBM20-4.12, and vehicle. (**D** and **F**) Editing efficiency at humanized *RBM20* locus, detected from whole heart
859 DNA samples. (**E**, **G**, and **H**) Editing efficiency at humanized *RBM20* locus, detected from left median lobe liver
860 DNA samples. (**I**) RNA/DNA ratio of fully edited sequence and partially edited sequence outcomes for humanized
861 *hRBM20*^{R634Q}*/hRBM20*$^{+}$ mice treated with PE-hRBM20-4.9. For D to E, each dot represents one animal. For F and
862 G, statistical significance was calculated using one-way ANOVA with Tukey's multiple comparisons test. $^{**}P <$
863 0.01, $^{****}P < 0.0001$.